

1 Seismic data analysis for subglacial lake D2 beneath David Glacier, 2 Antarctica

3 Hyeontae Ju^{1,2}, Seung-Goo Kang³, Yeonjin Choi³, Sukjoon Pyun², Min Je Lee³, Hoje Kwak⁴, Kwansoo
4 Kim¹, Yeadong Kim⁵, Jong Ik Lee³

5 ¹Center of Technology Development, Korea Polar Research Institute, Incheon 21990, Korea

6 ²Department of Energy Resource Engineering, Inha University, Incheon 22212, Korea

7 ³Division of Glacier & Earth Sciences, Korea Polar Research Institute, Incheon 21990, Korea

8 ⁴Unit of Antarctic Inland Research, Korea Polar Research Institute, Incheon 21990, Korea

9 ⁵Korea National Committee on Polar Research, Incheon 21990, Korea

10

11 *Correspondence to:* Seung-Goo Kang (ksg9322@kopri.re.kr)

12 **Abstract.** Subglacial lakes beneath Antarctic glaciers are pivotal in advancing our understanding of cryosphere dynamics,
13 basal hydrology, and microbial ecosystems. We investigate the internal structure and physical properties of Subglacial Lake
14 D2 (SLD2), which is located beneath David Glacier in East Antarctica, using seismic data acquired during the 2021/22 austral
15 summer. The dataset underwent a comprehensive processing workflow, including noise attenuation, velocity analysis, and pre-
16 staekprestack time migration. MigratedThe migrated seismic sections revealed distinct reverse- and normal-polarity reflections
17 at the glacier–lake and lake–bed interfaces, respectively. We compared the synthetic seismogram generated through wave
18 propagation modelling-basedmodeling on the basis of our structural interpretation of the migrated sections with the field data
19 to validate the subglacial lake structure inferred from the seismic data. This confirmed at that the water column thickness
20 ranged from aroundapproximately 53 to 82 m and delineated the broader structure of the subglacial lake. AlsoAdditionally,
21 discontinuous reflections detected onin seismic sections transverse to the ice flow were interpreted as scour-like feature
22 surfaces formed by ice movement. ComparisonA comparison with airborne ice-penetrating radar (IPR) data acquired in 2018
23 further supported the consistency of the ice thickness estimates. Notably, a steeply dipping bedrock boundary identified along
24 profile 21YY provided a more precise definition of the lateral extent of SLD2 than was possible usingwhen IPR data alone
25 were used. Collectively, these findings enhance our understanding of subglacial lake environments and inform the selection of
26 future drilling sites for in situ sampling.

27 1 Introduction

28 Subglacial lakes beneath the Antarctic Ice Sheetice sheet are typically overlain by glaciers several kilometers thick and have
29 remained isolated from direct atmospheric and solar influences for millions of years, creating extreme environments
30 characterized by low temperatures (Thoma et al., 2010) and high pressures (Tulaczyk et al., 2014). With increasing scientific
31 interest, subglacial lakes have become a focal point for studies related to the Antarctic paleoclimate, as inferred from lake

32 sediments, as well as investigations into microbial life in polar ecosystems (Bell et al., 2007, 2011; Bentley et al., 2009;
33 Christner et al., 2014; Engelhardt et al., 1990; Priscu and Christner, 2003; Rose, 1979; Wingham et al., 2006). Subglacial lakes
34 in Antarctica are generally categorized as either stable or active. Approximately 80% of subglacial lakes in Antarctica are
35 classified as stable subglacial lakes. These closed systems do not exhibit significant surface elevation changes and where
36 subglacial water remains largely isolated, with minimal exchange due to slow and stable recharge and discharge cycles. The
37 remaining 20% are classified as active subglacial lakes, which exhibit surface elevation changes due to episodic water drainage
38 and refilling events (Livingstone et al., 2022). Additionally, these lakes influence glacier dynamics by reducing basal friction,
39 facilitating ice flow, and potentially accelerating calving events. Such active lakes can reduce basal friction as they expand,
40 thereby facilitating glacier flow and, in some cases, accelerating calving processes, ultimately influencing glacier dynamics
41 (Bell et al., 2007; Stearns et al., 2008; Winsborrow et al., 2010). Characterizing subglacial lakes is essential for understanding
42 cryospheric processes, reconstructing past climate conditions, and assessing the potential for life in isolated, extreme
43 environments.

44 The sampling of subglacial lake water, sediments, and microbial communities is critical to address these scientific objectives.
45 However, successful sampling requires careful selection and characterization of the drilling site. Airborne ice-penetrating radar
46 (IPR) surveys are commonly employed at regional scales to detect potential subglacial lakes suitable locations for drilling
47 (Christianson et al., 2012; Lindzey et al., 2020; Yan et al., 2022). However, due to signal attenuation in water, IPR surveys are
48 limited in resolving the internal structure of subglacial lakes. To overcome this limitation, seismic surveys have been conducted
49 at potential subglacial lake candidates identified from IPR surveys. During such surveys, P-waves propagate through the water
50 column and are partially reflected at the lake–bed interface because of contrasts in acoustic impedance. Analyzing these
51 reflected waves enables detailed delineation of the water column and underlying substrate, thereby informing optimal drilling
52 locations (Brisbourne et al., 2023; Filina et al., 2008; Horgan et al., 2012; Woodward et al., 2010).

53 As such, numerous studies have utilized seismic surveys to investigate the characteristics of subglacial lakes, including
54 Subglacial Lake Ellsworth, Subglacial Lake Whillans, and Subglacial Lake CECs. Subglacial Lake Ellsworth, located beneath
55 2,930–3,280 m of glacial ice in West Antarctica, was the subject of a seismic survey during the austral summer of 2007–08.
56 This survey revealed spatially variable ice thickness and a lake water column ranging from 52 to 156 m, which guided the
57 identification of an optimal drilling location (Smith et al., 2018; Woodward et al., 2010). Subglacial Lake Whillans lies beneath
58 approximately 800 m of ice. Seismic observations conducted during the 2010/11 field season revealed water columns
59 extending over a 5 km segment of the survey profile, with a maximum thickness of less than 8 m. The glacier bed was
60 predominantly composed of soft sediments, and localized zones with shallow water columns (< 2 m) were also identified
61 (Horgan et al., 2012). Subsequent drilling in the summer of 2012/13 confirmed the presence of microbial life in both the water
62 and sediment samples (Christner et al., 2014). Subglacial Lake CECs (SLCECs), located beneath 2653 m of ice at the Rutford–
63 Institute–Minnesota Divide in West Antarctica, were investigated through seismic surveys conducted in the 2016/17 and
64 2021/22 seasons. These surveys revealed a maximum water column thickness of 301.3 ± 1.5 m and clastic sediments up to 15

65 m thick covering the lakebed. While the lake center was relatively flat, significant topographic variability was observed near
66 the lake margins (Brisbourne et al., 2023).

67 We have initiated subglacial lake research beneath David Glacier, the closest major glacier to Jang Bogo Station in East
68 Antarctica. Satellite altimetry has identified six subglacial lakes in this region (Smith et al., 2009; Wright and Siegert, 2012).
69 During the 2016/17 austral summer, an airborne IPR survey was conducted over the region encompassing Subglacial Lake D1
70 (SLD1) and Subglacial Lake D2 (SLD2) (Lindzey et al., 2020). A subsequent high-resolution IPR survey was carried out
71 during the 2018/19 field season, focusing solely on SLD2 (Frémand et al., 2023; Ju et al., 2024b5). The combined results of
72 the two surveys revealed moderately enhanced radar bed echoes relative to the surrounding area, specularity values (>0.4), a
73 depressed basal elevation (≤ -350 m), and a low hydraulic gradient ($\leq 0.84^\circ$), collectively indicating a high potential for the
74 presence of subglacial water beneath SLD2. Seismic Building upon these observations, Ju et al. (2025) subdivided the
75 previously identified single subglacial water body at SLD2, as detected by ICESat altimetry, into three smaller subglacial lakes:
76 SLD2-A, SLD2-B, and SLD2-C. Among these, SLD2-A represents the largest areal extent, and targeted seismic surveys were
77 employed conducted over this area to investigate the structure of obtain high-resolution information on the lake further depth
78 and basal structure. In the 2019/20 season, an initial seismic campaign identified the glacier thickness and suggested the
79 presence of the lake; however, the data quality was compromised by surface crevasse noise and a lack of adequate fold coverage,
80 limiting detailed interpretation. A refined seismic survey with 8-fold coverage was conducted during the 2021/22 season to
81 address these issues.

82 In this study, we present a detailed analysis of the physical and structural properties of SLD2-A using seismic data acquired
83 during the 2021/22 campaign. We first describe the seismic data processing workflow, including noise attenuation, amplitude
84 correction, and pre-stack prestack time migration. The final results reveal seismic reflections corresponding to the glacier—
85 lake and lake—bed interfaces. Subsequently, the The seismic interpretation is subsequently validated through a comparison
86 with synthetic seismograms, and a quantitative analysis is performed to determine the key structural characteristics of SLD2—
87 A, including the ice thickness, water column thickness, and basal structure of the lake.

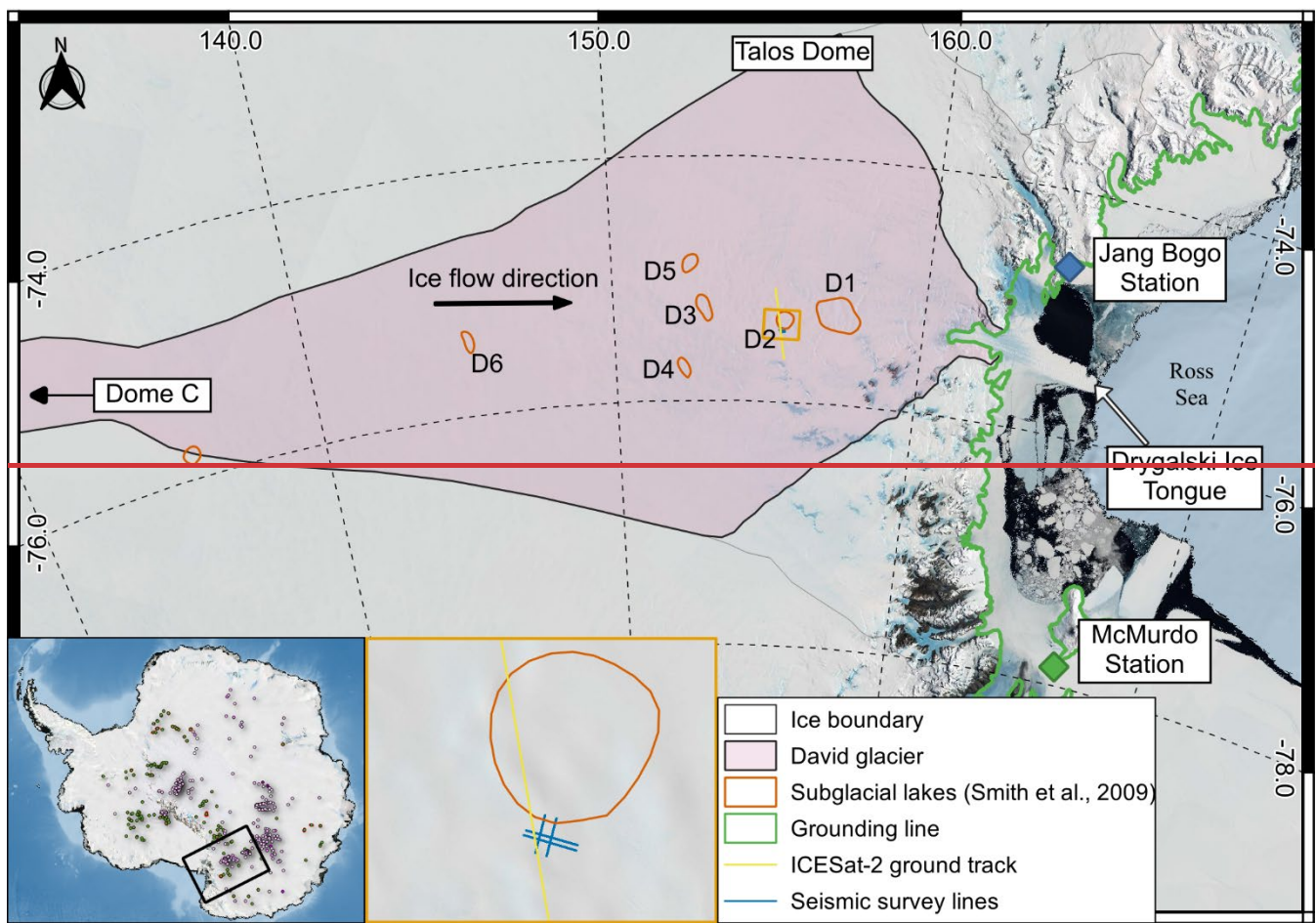
88 2 Subglacial Lake D2 Beneath David Glacier in Antarctica

89 2.1 David Glacier

90 David Glacier, located in Victoria Land, East Antarctica, originates from the Dome C and Talos Dome regions and flows
91 seaward through the Drygalski Ice Tongue (Fig. 1). The mass balance of the glacierglaciers from 1979 to 2008 has been
92 estimated at 7.5 ± 0.4 Gt yr $^{-1}$ (Rignot et al., 2019), while the mean ice discharge over the more extended period from 1979 to
93 2017 was reported to be approximately 9.7 Gt yr $^{-1}$ (Frezzotti et al., 2000; Rignot et al., 2019). These estimates suggest that ice
94 discharge exceeds net accumulation, indicating a negative mass balance and implying that David Glacier has contributed to
95 global sea level rise According to Smith et al. (2020), satellite altimetry observations from ICESat-1 and ICESat-2 (2003–2019)
96 indicate that the grounded portion of David Glacier experienced a mass gain of 3 ± 2 Gt yr $^{-1}$, whereas the adjacent ice shelves

97 exhibited a mass loss of -1.6 ± 1 Gt yr $^{-1}$. Although the overall mass balance of David Glacier currently appears stable, it
98 remains uncertain how long this stability can be maintained.

99



100

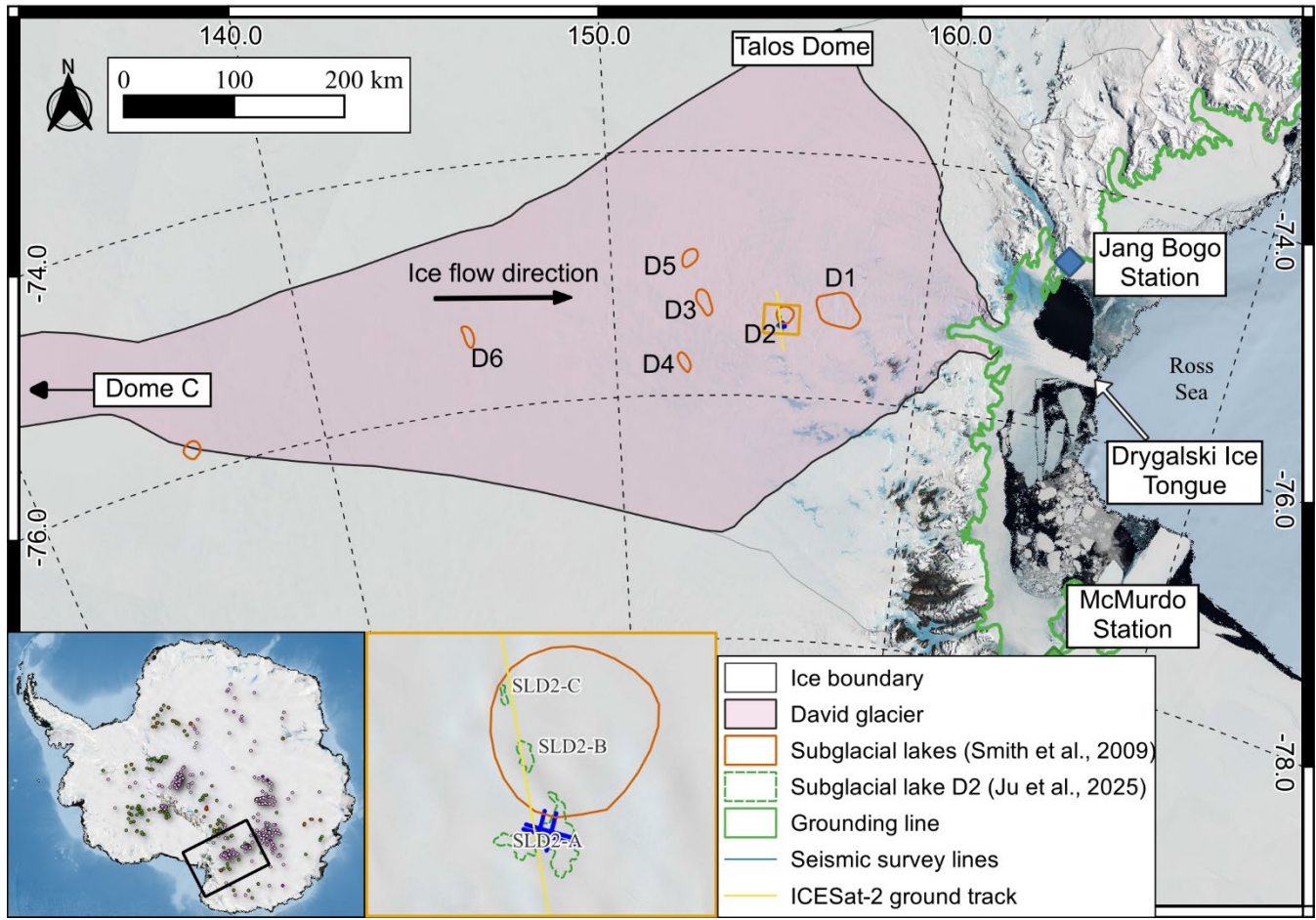


Figure 1: Locations of subglacial lakes D1–D6 in the David Glacier region, Victoria Land, Antarctica (EPSG: 4326–WGS84).

103

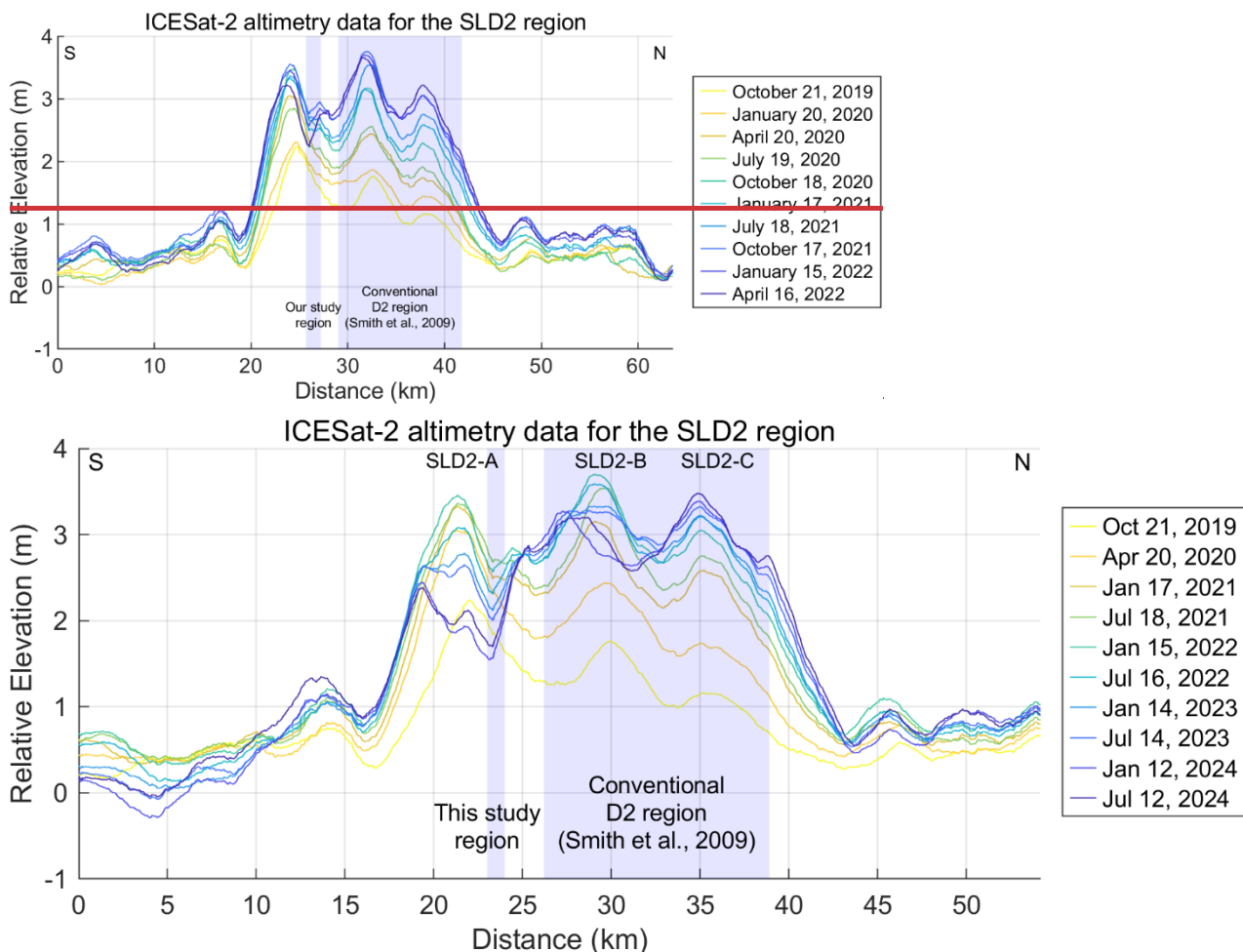
104 2.2 Subglacial Lake D2

105 Subglacial lakes in Antarctica are generally categorized as either stable or active. Approximately 80% of subglacial lakes in
 106 Antarctica are classified as stable subglacial lakes. These closed systems do not exhibit significant surface elevation changes,
 107 and where subglacial water remains largely isolated, with minimal exchange due to slow and stable recharge and discharge
 108 cycles. The remaining 20% are classified as active subglacial lakes, which exhibit surface elevation changes due to episodic
 109 water drainage and refilling events (Livingstone et al., 2022).

110 Among the six subglacial lakes (D1–D6) identified beneath David Glacier via satellite altimetry (Smith et al., 2009; Wright
 111 and Siegert, 2012), SLD2 was observed to have experienced a drainage event between 2003 and 2008 based on the basis of
 112 ICESat altimetry data (Smith et al., 2009). Since the drainage event, a continuous increase in surface elevation over SLD2 has
 113 been observed, indicating water refilling, as detected from CryoSat-2 altimetry data (2013–2017) (Siegfried and Fricker, 2018)

114 and more recently from ICESat-2 observations (2019–2024) (Fig. 2). Figure 2 shows elevation changes relative to April 2019,
115 indicating surface uplift through January 2022. After this period, the surface elevation remained stable in the region originally
116 delineated as SLD2 (by Smith et al., 2009), whereas the seismic survey region experienced a decreased elevation trend
117 was observed in the SLD2-A region (Ju et al., 2025). These patterns of elevation change strongly suggest that SLD2 is an
118 active subglacial lake, with cyclic drainage and refilling likely contributing to the presence of subglacial sediments.
119

120



122 Figure 2: Glacier surface elevation changes derived from ICESat-2 altimetry between 22 April 2019 and 12 July 2024. The X-axis
123 corresponds to the 22 April 2019 dataset, and all subsequent elevation changes are referenced to this date. The light blue shaded
124 region indicates the spatial overlap between the conventional SLD2 region identified by Smith et al. (2009) and our study region.

125

126 Airborne IPR surveys were conducted during the 2016/17 and 2018/19 austral summer seasons to better constrain the lake's
127 extent and basal conditions. These surveys of SLD2, airborne IPR survey data from 2016/17 (Lindzey et al., 2020) and 2018/19
128 (Ju et al., 2025) field campaigns indicate that glacier surface elevations in the SLD2 region range from approximately 1820 to

129 1940 m, with ice thicknesses varying between 1685 and 2293 m. Furthermore, the observations of moderately enhanced radar
130 bed echoes relative to the surrounding area, elevated specularity values (>0.4), depressed basal elevations (≤ -350 m), ~~350~~
131 ~~m), the presence of a Bain-like topography, a lower hydraulic head than the surroundings, and low hydraulic gradients ($\leq 0.84^\circ$)~~
132 collectively suggest a high potential for the presence of subglacial water beneath SLD2. (Frémard et al., 2022; Ju et al., 2024b;
133 Lindzey et al., 2020).

134 3 Method

135 3.1 Seismic survey

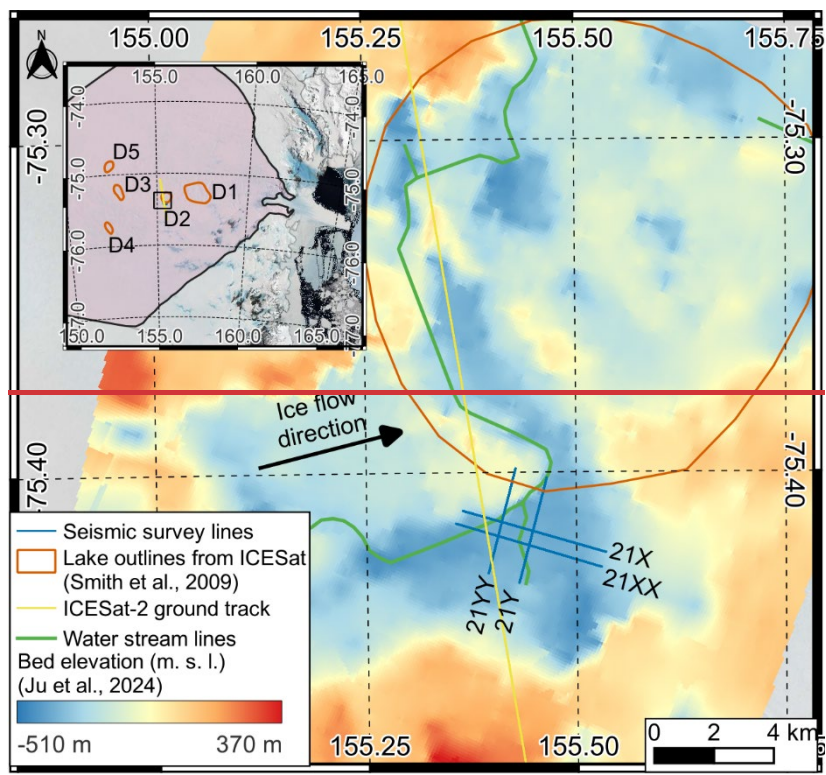
136 As previously noted, the internal structure and water column of subglacial lakes cannot be fully resolved using IPR alone
137 because of signal attenuation in water. Accordingly, a seismic survey was conducted within the candidate SLD2-A region
138 identified from IPR data to investigate the structure of the subglacial lake more precisely. A

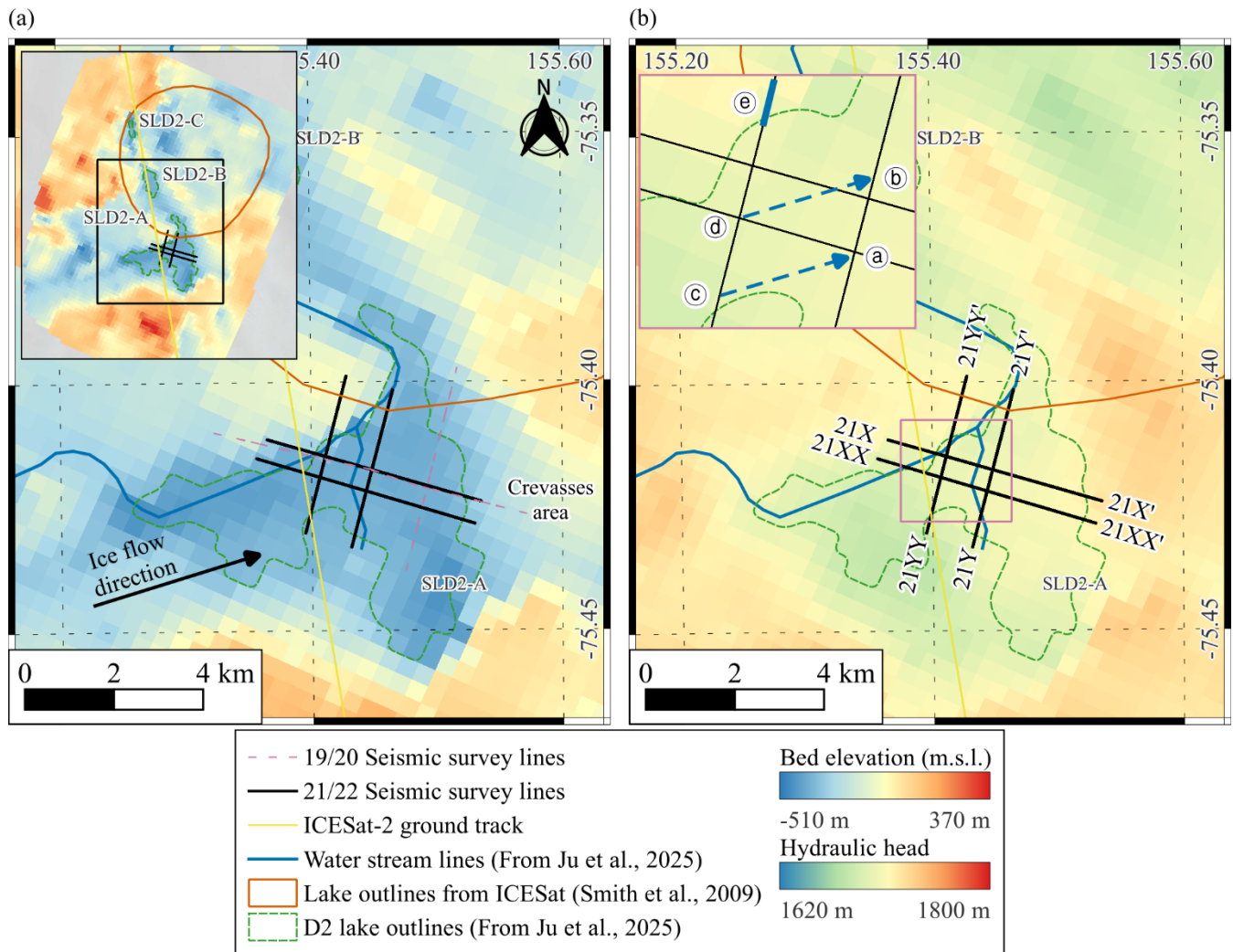
139 ~~During the 2019/20 austral summer, a preliminary seismic survey was conducted during the 2019/20 austral summer over the~~
140 ~~SLD2-A region to evaluate the potential presence of a subglacial lake and to obtain initial information on its structural~~
141 ~~characteristics. Owing to limited field time and equipment constraints, the fold of coverage for all survey lines was restricted~~
142 ~~to 1, and all shot points were aligned near surface crevasses. Consequently, the acquired seismic data were significantly~~
143 ~~contaminated by strong linear coherent noise associated with crevasses, which severely degraded the signal quality of key~~
144 ~~reflectors, particularly reflections from the subglacial lake–bedrock interface. In addition, explosives are deployed within~~
145 ~~shallow boreholes (< 20 m depth), and owing to the absence of proper backfilling and the rapid timing of detonation, poor~~
146 ~~coupling between the explosives and the borehole walls further reduces energy transmission efficiency, resulting in overall~~
147 ~~low-quality reflection signals (Ju et al., 2024). As a result, due to the limitations of single-fold acquisition, stacking was not~~
148 ~~feasible, resulting in a low signal-to-noise ratio (SNR) and the presence of dominant coherent noise, rendering the seismic~~
149 ~~dataset unsuitable for quantitative structural interpretation. Nevertheless, the preliminary survey qualitatively confirmed both~~
150 ~~the glacier thickness and beneath SLD2-A and suggested the presence of subglacial water, providing critical guidance for~~
151 ~~baseline information that guided the methodology and survey design of the subsequent detailed survey seismic campaign~~
152 conducted during the 2021/22 season.

153 For the refined survey, seismic acquisition lines were planned using bed topography derived from the IPR and surface elevation
154 data from satellite altimetry. A total of four seismic lines were ~~deployed acquired~~ and designated 21X, 21Y, 21XX, and 21YY
155 (Fig. 3). Lines 21X and 21XX, oriented approximately 52° relative to the ice flow direction, are situated at an average surface
156 elevation of 1894 ± 13 m. Lines 21Y and 21YY, oriented approximately -30° in the ice flow direction, lie at an average
157 elevation of 1887 ± 16 m. All lines traverse regions of minimal topographic relief, with average surface slopes of approximately
158 0.5° , indicating a relatively flat and stable glacier surface. The lengths of the 21X/21XX and 21Y/21YY lines are
159 approximately 5 km and 3.5 km, respectively. Seismic acquisition for lines 21X and 21Y was conducted using 8-fold coverage

160 to increase the resolution, whereas lines 21XX and 21YY were acquired with 4-fold coverage due to time constraints during
161 the survey. The additional acquisition parameters are summarized in Table 1.

162





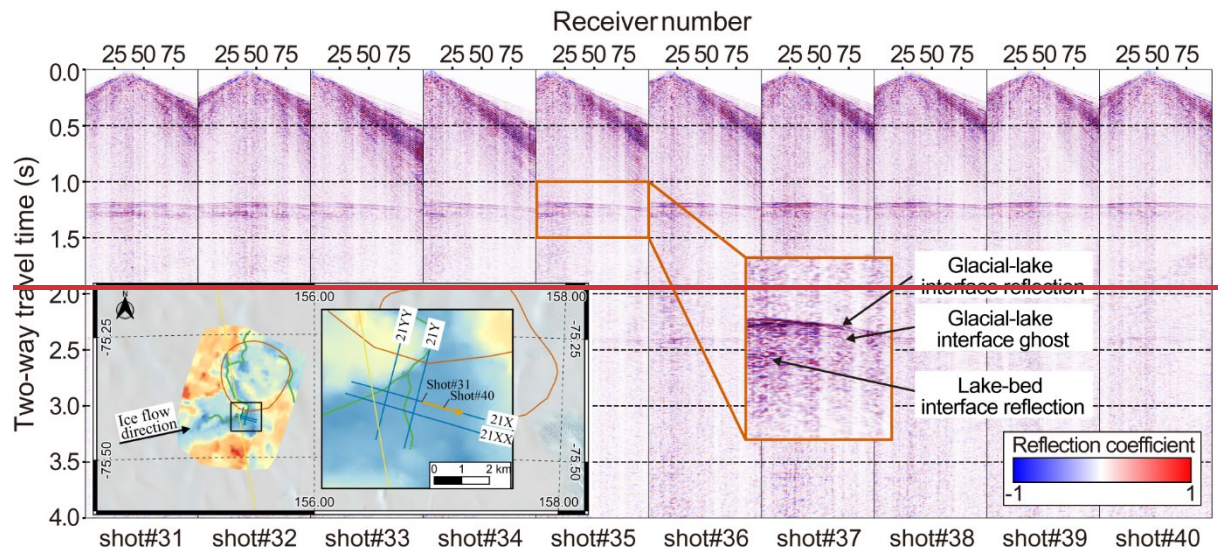
164
165 **Figure 3: 21/22 Seismic survey layout (blue/black lines) overlaid on (a) bed elevation and (b) hydraulic head data from IPR results**
166 **(Ju et al., 2024b).**

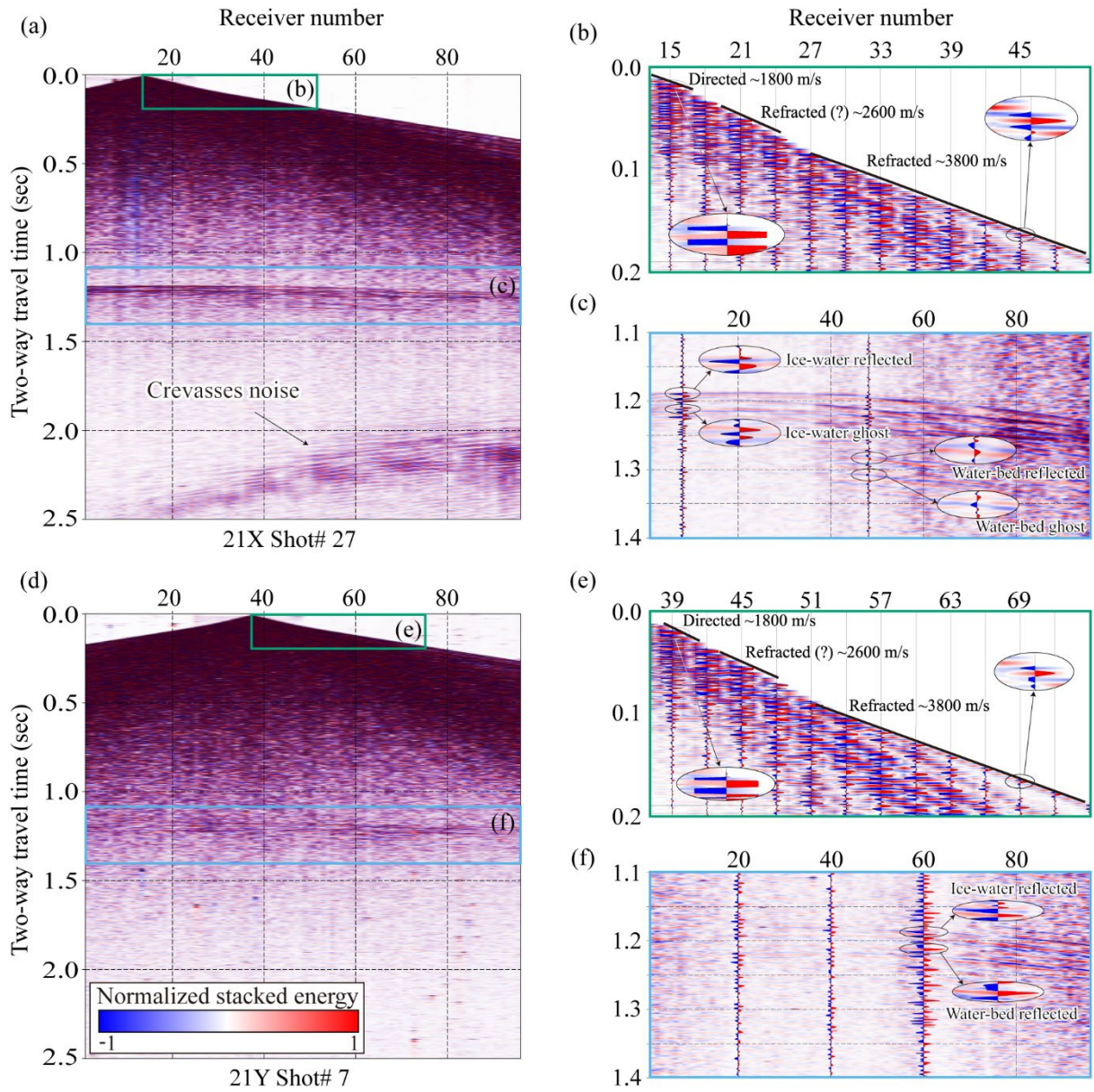
167
168
169
170
171
172
173 **Table 1: Parameters of the active-source seismic survey.**

Survey Parameters	Survey lines			
	21X line	21Y line	21XX line	21YY line
Line length (km)	5	3.5	5	3.5
Fold	8	8	4	4
Shot interval (m)	90	90	180	180
Number of shots	56	40	28	20
Receiver channels		96		
Receiver interval (m)		15		
Recording time (s)		4		
Record peak frequency (kHz)		1		
Record sampling rate (ms)		0.25		
Survey time (days)		34		
Survey crew size	Hot water drilling (3), Seismic (6)			

174

175 Before the seismic survey, a ground-penetrating radar (GPR) survey was used to identify the firn transition zone at depths of
 176 approximately 20–22 m. To enhance seismic signal transmission, 1.6 kg of pentaerythritol tetranitrate (PETN) explosives were
 177 emplaced at depths of 25–30 m using hot water drilling techniques. A total of 144 shots were deployed across the four survey
 178 lines. Given the snow-covered glacier surface, Georods were used instead of conventional spike-type geophones to increase
 179 signal detection efficiency (Voigt et al., 2013). Each Georod houses four geophone elements in a 0.6 m-long cylindrical array,
 180 producing a single output by summing the inputs from all the elements. Compared with traditional geophones, this
 181 configuration improves coupling and detection performance in snow-dominated environments (Ju et al., 2024a). Figure 4
 182 presents shot ~~gathers #31–40~~ gather #27 from line 21X. ~~Orange arrows indicate the positions of the corresponding and~~ shot
 183 ~~points along the 21X profile. Within gather #7 from line 21Y. In~~ these shot gathers, ~~the velocity of the direct wave is estimated~~
 184 ~~to be approximately 1800 m/s, and the refracted wave velocity is approximately 3800 m/s. First-arrival analysis of the direct~~
 185 ~~wave indicates a normal polarity, confirming the source waveform polarity. A prominent negative polarity reflection is~~
 186 ~~observed~~ at a two-way travel time (TWT) of approximately 1.2 s ~~is 2 s~~, interpreted as the glacier–lake interface, ~~followed by~~.
 187 ~~Approximately 25–30 ms later, a ghost reflection 20–30 ms later. A second with normal polarity appears. A subsequent~~
 188 ~~reflection, observed at approximately 1.3 s TWT of 1.3 s, showing normal polarity, is attributed to the lake–bed interface. In~~
 189 ~~some end, followed by its negative polarity ghost reflection 25–30 ms later. In~~ shot ~~gathers, such as shot~~ gather #33, linear 27,
 190 ~~noise signals interfere with the glacier–lake interface signal originating from crevasses becomes apparent from approximately~~
 191 ~~2 s TWT. As the distance to the crevasses decreases, this noise increasingly overlaps with the primary reflection arrivals,~~
 192 ~~complicating the~~ interpretation.
 193





196
197 **Figure 4: Raw shot records from seismic lines 21X (a) and 21Y (d). Panels (b) and (e) are zoomed-in views of the early arrival window**
198 **(0.0–0.2 s) from panels (a) and (d), respectively, used to calculate the apparent velocities of the direct and refracted waves. These**
199 **panels highlight that the first arrivals of both the direct wave (clipped for display) and the refracted wave exhibit positive polarity.**
200 **The direct wave, propagating through the upper firn layer (0–25 m depth), shows an apparent velocity of direct waves, approximately**
201 **1800 m/s, while the refracted wave traveling through glacier ice has an apparent velocity of reflections approximately 3800 m/s.**
202 **Panels (c) and (f) are zoomed-in views of the deeper arrivals (1.1–1.4 s) from panels (a) and (d), respectively. Reflections from the**
203 **ice–water interface exhibit negative polarity, whereas those from the water–bed interface display positive polarity.**

204 **Raw shot records from seismic lines 21X (a) and 21Y (d). (b) Zoomed-in view of the early arrivals (0.0–0.2 s) in panel (a), highlighting**
205 **direct and refracted waves. (e) Zoomed-in view of deeper arrivals (1.1–1.4 s) in panel (a). (c) Zoomed-in view of the early arrivals**
206 **(0.0–0.2 s) in panel (d). (f) Zoomed-in view of deeper arrivals (1.1–1.4 s) in panel (d). In panels (b) and (e), the direct wave**

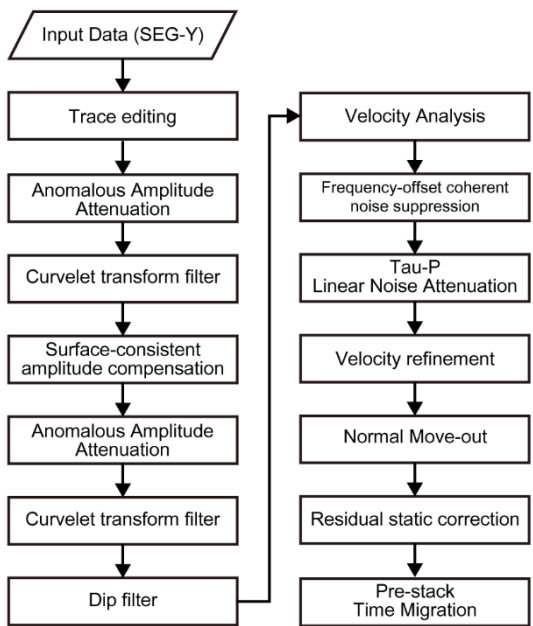
207 corresponding to the upper firn layer (0–25 m depth) – propagates with an apparent velocity of approximately 1800 m/s, while the
208 refracted wave through glacier ice exhibits an apparent velocity of about 3800 m/s. In panels (c) and (f), reflections from the ice–
209 water interface exhibit negative polarity, while those from the water–bed interface show positive polarity.

210

211 3.2 Seismic data processing

212 Although seismic data acquired from glaciers share processing similarities with those of land-based surveys, glaciological
213 factors, such as surface cracks, crevasses, and strong winds, introduce substantial noise that can degrade data quality (Johansen
214 et al., 2011; Zechmann et al., 2018). Among these factors, linear noise generated by crevasses is particularly detrimental, often
215 obscuring key reflections (Dow et al., 2013). Hence, the glacier seismic data underwent multiple data processing sequences
216 focused on linear noise removal (Fig. 5). ~~Acquisition~~ geometry ~~setup~~ was ~~performed~~~~added~~ to the data using the raw data and
217 geometry information. Multiple data processing and noise removal processes were then carried out to increase the signal-to-
218 noise ratio (SNR).

219



220
221 **Figure 5: Schematic of the seismic data processing workflow based on the Omega geophysical data processing platform~~SLB~~,
222 including noise attenuation, amplitude correction, velocity analysis, and ~~pre-stack~~~~prestack~~ time migration.**

223

224 The initial processing involved anomalous amplitude attenuation (AAA), implemented via a spatial median filter. This step
225 targets outlier amplitudes within a defined frequency band, attenuating anomalous signals through interpolation across
226 neighboring traces. A curvelet transform-based filter was subsequently applied to remove coherent noise. Curvelet
227 decomposition enables the separation of signals ~~based on~~ the basis of dip angle and scale, allowing for the selective removal

228 of ground roll and other coherent noise components that differ in dip from true reflections (Oliveira et al., 2012). In this study,
229 linear coherent noise at later arrival times (>2.0 s) was effectively removed using this method.

230 Surface-consistent amplitude compensation (SCAR) and surface-consistent deconvolution were employed to normalize the
231 amplitude variability across shot gathers. These steps were followed by a second round of AAA and curvelet filtering to
232 suppress artifacts introduced during the compensation and deconvolution stages. Dip filtering was also applied to eliminate
233 spurious hyperbolic arrivals, which were manually identified and removed.

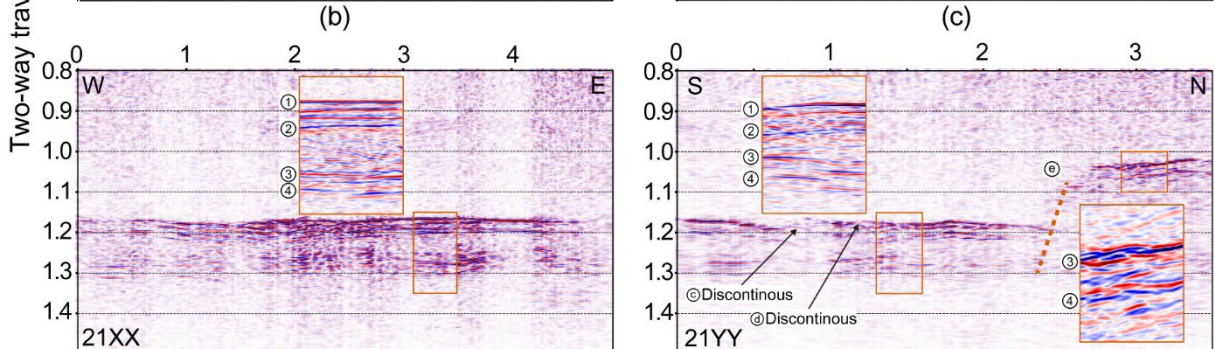
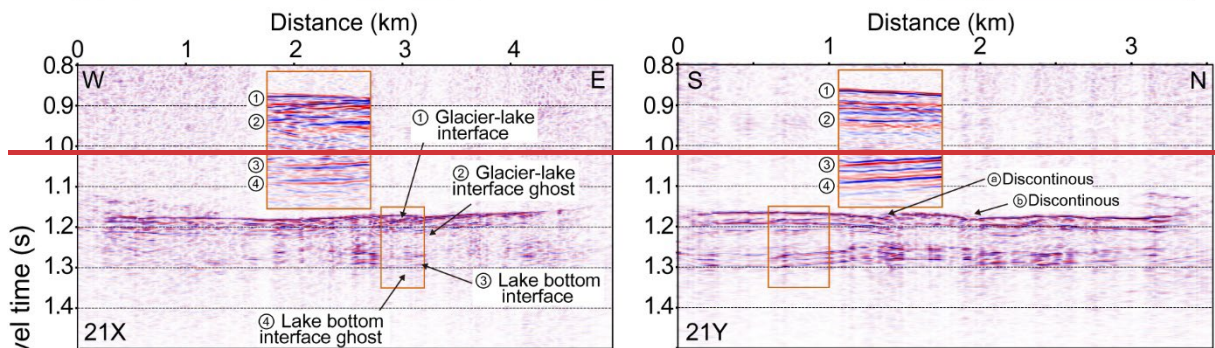
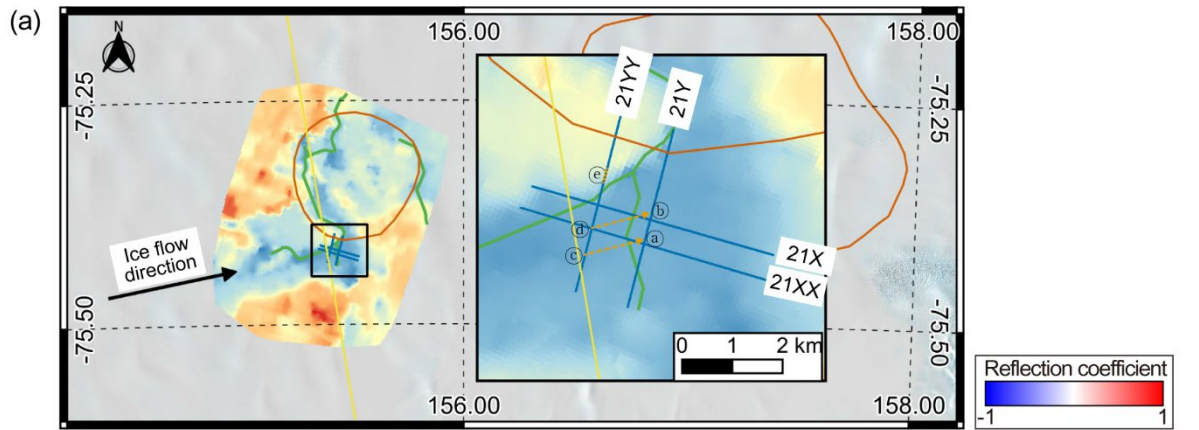
234 Velocity analysis was conducted at intervals of 40 common ~~mid points~~midpoints to construct a migration velocity model.
235 Frequency-offset coherent noise suppression (FXCNS) was used to attenuate linear-related noise, followed by Tau-p linear
236 noise attenuation (LNA), effectively reducing the noise associated with crevasse scattering. The final processing steps included
237 velocity model refinement, normal move-out (NMO) correction, and ~~pre-stack time migration (PSTM)~~prestack time migration
238 (PSTM). The specific parameters employed for data processing, as well as the intermediate outcomes at each processing stage,
239 are provided in the supplementary information (S1).

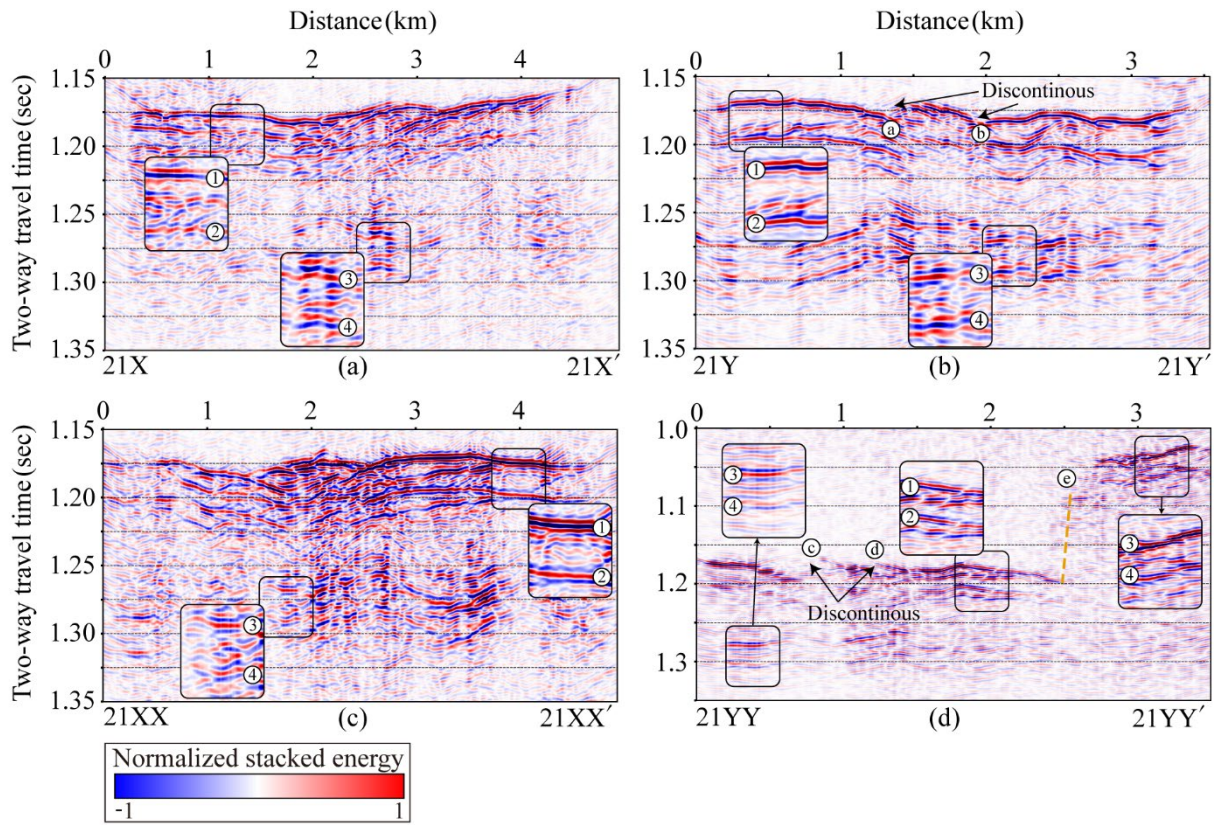
240 To increase imaging accuracy, a residual static correction was applied before migration using glacier surface elevation data.
241 The final migrated seismic section was produced using Kirchhoff PSTM. The migrated data has ~~sve~~ a center frequency of
242 approximately 180 Hz. Assuming seismic wave velocities between 1395 m/s and 3800 m/s, the corresponding vertical
243 resolutions, which are calculated using the quarter-wavelength criterion, range from approximately 2.01 m to 5.27 m. This
244 resolution is adequate for imaging SLD2.

245 **4 Seismic data processing results**

246 Figure 6 presents the PSTM results for the four seismic survey lines. On line 21X (Fig. 6b6a), a strong, laterally continuous
247 reflection with reverse polarity is observed at 0.3–4.8 km along the profile, and the two-way travel time (TWT) is
248 approximately 1.~~19~~15–1.~~18~~18 s. This reflection is interpreted as the glacier–lake interface (①). Approximately 25–30 ms below
249 this horizon, a normal-polarity reflection (②) appears, likely representing a ghost signal associated with the primary glacier–
250 lake reflection. A deeper normal-polarity reflection is observed within 2.~~5~~1.9–3.1 km at TWTs of 1.~~25~~1.27–1.~~29~~29 s (③),
251 which is interpreted as the lake–bed interface. This is followed by a reverse-polarity reflection 25–30 ms later (④), which is
252 presumed to be the corresponding ghost of the lake–bed interface.

253





256 **Figure 6: PSTM seismic sections for lines (ba) 21X, (eb) 21Y, (ec) 21XX, and (ed) 21YY prior to ghost removal. Ghost reflections**
 257 **appear 25–30 ms beneath the glacier–lake and lake–bed interfaces due to the 25 m source depth.**

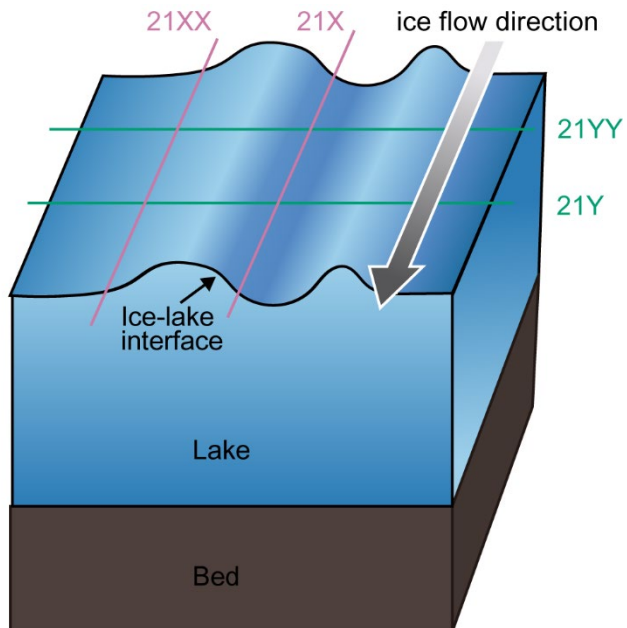
258
 259 In line 21Y (Fig. 6e6b), similar features are observed. A reverse-polarity reflection, interpreted as the glacier–lake interface
 260 (①), is observed within 0.1–3.2 km at TWT 1.4917–1.18 s, with its ghost reflection (②), ~~exhibiting which exhibits~~ normal
 261 polarity, ~~appearing and appears~~ 25–30 ms later. A normal-polarity reflection within 0.1–3.2 km at a TWT of 1.26–1.2927 s is
 262 interpreted as the lake–bed interface (③), followed by a reverse-polarity ghost signal (④). Additionally, discontinuous
 263 reflections interpreted as subglacial scour-like features (SLF) are visible at approximately 1.43 km (⑤) and 1.9 km (⑥) along
 264 line 21Y at TWT 1.4918 s (black arrows in Fig. 6e6b). These features may be associated with glacial erosion of the underlying
 265 substrate.

266 In line 21XX (Fig. 6e6c), a reverse-polarity reflection, interpreted as the glacier–lake interface (①), is observed within 0–
 267 4.23 km at a TWT of 1.4917–1.2018 s. This reflection is followed 25–30 ms later by a normal-polarity reflection (②), which
 268 is considered the ghost of the primary glacier–lake interface. Further down the section, a normal-polarity reflection (③) within
 269 1.9–4.2 km at a TWT of 1.2725–1.2928 s is interpreted as the lake–bed interface, followed by its ghost reflection (④) 25–30
 270 ms later.

271 On line 21YY (Fig. 6e6d), the glacier–lake interface (①) is marked by a strong, flat, reverse-polarity reflection at 0–2.4 km
272 and a TWT of 1.17–1.4920 s, followed by its normal-polarity ghost (②) 25–30 ms below. Lake–bed interface reflections (③)
273 are observed within 0.42–2.4 km at TWTs of 1.27–1.3029 s, followed by a reverse-polarity ghost (④) 25–30 ms later. Within
274 2.4–2.55 km and TWTs of 1.08–1.2717 s, no coherent reflection is visible due to the steeply dipping bed topography, as
275 indicated by the dashed orange line in Fig. 6e6d. Within 2.55–3.54 km and a TWT of 1.0203–1.409 s, a stair-step-shaped
276 reflection at the glacier–bed interface (③) is identified, followed by its reverse-polarity ghost (④). Additionally, similar to
277 observations on line 21Y, discontinuous reflections interpreted as *seourSLF* surfaces appear at 0.7 km (⑤) and 1.2 km (⑥)
278 along line 21YY at TWT 1.4918 s (black arrows in Fig. 6e6d).

279 The discontinuous reflection signals identified on lines 21Y and 21YY are spatially aligned along the ice flow direction when
280 projected laterally (Fig. 6a3, dashed orangeblue arrow). This alignment suggests that the observed discontinuities correspond
281 to a subglacial *seourSLF* surface formed by glacial motion. The *seour featureSLF* is visible predominantly on lines 21Y and
282 21YY, which are oriented more perpendicularly to the ice flow direction, thereby enhancing the expression of lateral subglacial
283 variability. In contrast, lines 21X and 21XX are more parallel to the ice flow, resulting in a foreshortened view of the subglacial
284 structures and a relatively flat appearance in the seismic sections (Fig. 7).

285



286

287 **Figure 7: Conceptual diagram illustrating the orientation of seismic survey lines relative to subglacial structures and the ice flow**
288 **direction, explaining the appearance of structural features in each line.**

289

290 **5 Comparison between field data and synthetic seismograms**

291 The depth estimation of subsurface structures from PSTM sections is subject to errors arising primarily from inaccuracies or
 292 uncertainties in the seismic velocity model. An inaccurate velocity model may result in erroneous positioning of reflection
 293 events, leading to misinterpretation of stratigraphic horizons (Herron, 2000; Yilmaz, 2001). Such limitations are typically
 294 mitigated through well-tie analysis, wherein seismic horizons are calibrated against borehole data. However, in the case of
 295 SLD2, no borehole data ~~is~~are currently available.

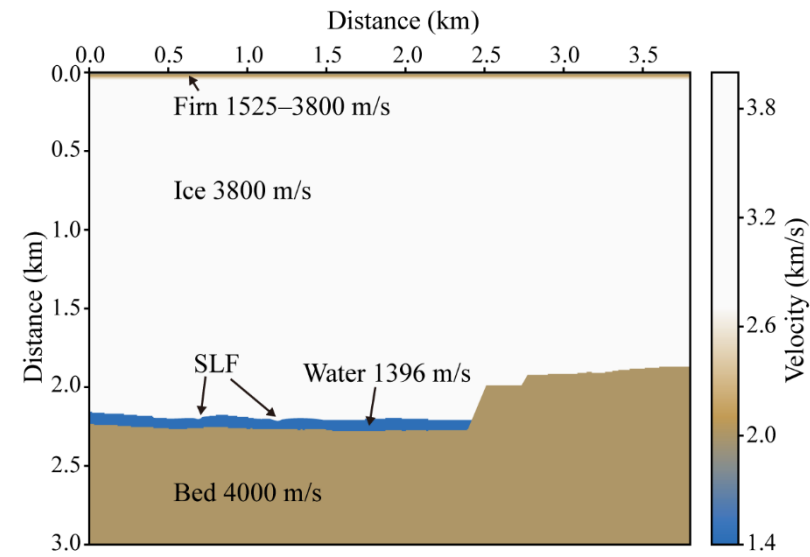
296 We validate the processed field data by performing a comparative analysis with synthetic seismograms to address this
 297 constraint. The forward modeling algorithms based on the staggered grid finite difference method in the time domain were
 298 used (Graves et al., 1996). The velocity model for this seismic modeling is constructed by structural information given by the
 299 seismic migration sections, integrating published values of P-wave velocities for firn, glacial ice, and subglacial water. P-wave
 300 velocities in firn vary from 1525 to 3800 m s⁻¹ because density increases with depth (Kirchner and Bentley, 1979; Picotti et
 301 al., 2015; Qin et al., 2024). Glacial ice has an average P-wave velocity of approximately 3800 ± 5 m s⁻¹ at -2 ± 2 °C (Kohnen,
 302 1974), while subglacial water has a velocity of ~~roughly~~^{approximately} 1396 ± 2 m s⁻¹ at -1.75 ± 0.25 °C, with a salinity less
 303 than 1 PSU (practical salinity units) (Thoma et al., 2010; Tulaczyk et al., 2014). Additionally, ~~is~~on line 21YY, the reflection
 304 polarity at the ice–bedrock interface ~~is~~appears as normal, indicating polarity, which indicates an increase in the acoustic
 305 impedance. In other words, this suggests that the P-wave velocity of the bedrock is ~~faster~~^{higher} than that of the overlying
 306 ~~glacial~~ ice. Therefore, the bedrock P-wave velocity was set to 4000 m s⁻¹. Using this information, a layered P-wave velocity
 307 model comprising firn, glacial ice, subglacial lakes, and bedrock was developed (Fig. 8). Forward modeling was then
 308 conducted using the Ricker wavelet, with acquisition parameters matching those used in the field survey (Table 2). ~~The same~~
 309 ~~seismic processing sequence~~^{We} applied ~~to~~^{just} the field data (Section 3.2, Fig. 5) was subsequently applied to migration step in
 310 case of the synthetic dataset to produce a PSTM image for comparison, as it is free of noise.

311

312 **Table 2: Parameters of the synthetic model.**

	Synthetic modeling parameters		
	Thickness (m)	Velocity (m/s)	Density (g/cm ³)
Model size	3.5 km (distance) x 3 km (depth)		
Source	Ricker wavelet (zero-phase), 60 Hz		
Receiver	25 m depth, 90-m interval		
Grid spacing	0 m depth, 15-m interval, 96 channel		
Sampling interval	0.5-m		
Layer parameters	0.1 ms		
Firn	100	1,525–3,800	0.3–0.917
Ice	1,887–2,221	3,800	0.917
Water	0–82±1.3	1,396	1.017
Bed	723–1,113	4,000	2.1

313



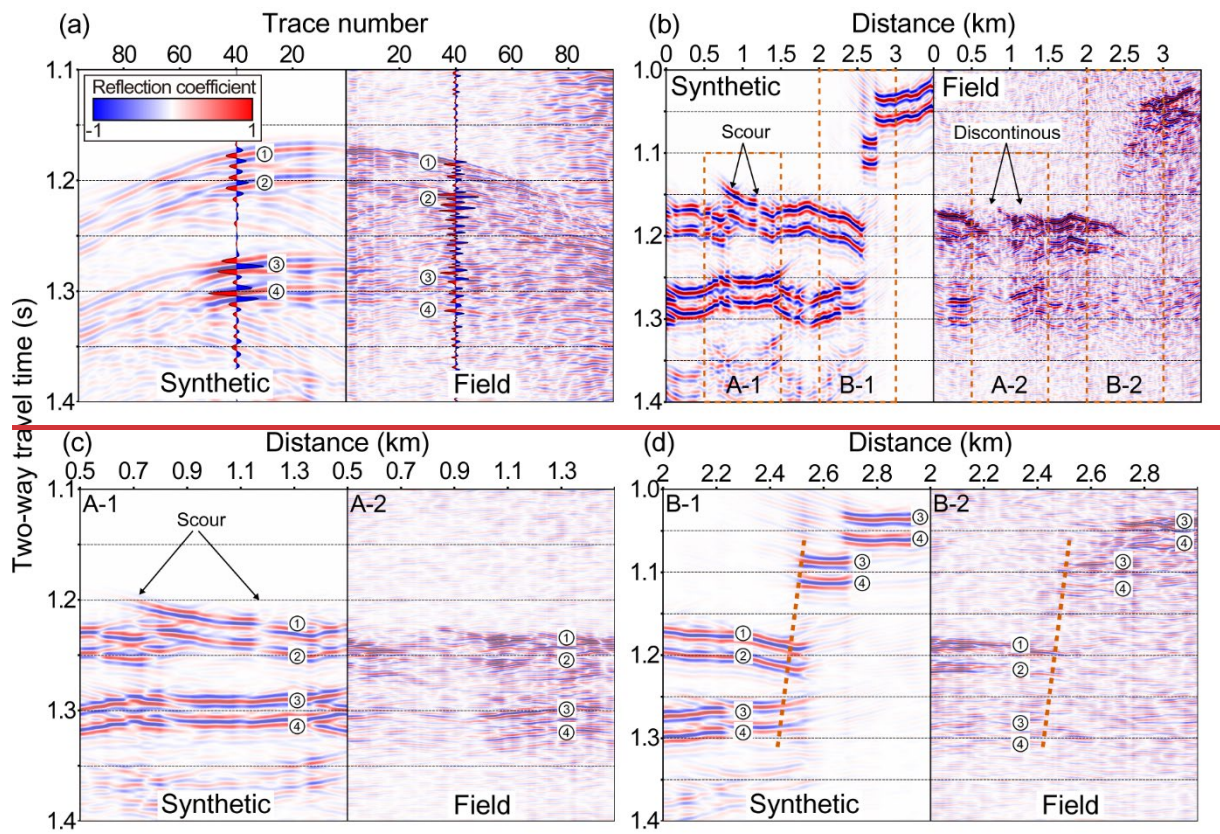
315 **Figure 8: P-wave velocity model used in forward modeling for line 21YY.** The upper ~100 m represents firn with velocities ranging
 316 from 1525 to 3800 m s⁻¹ (Kirchner and Bentley, 1979; Picotti et al., 2015; Qin et al., 2024). The ice below this depth has a velocity
 317 of 3800 ± 5 m s⁻¹ (Kohnen, 1974), and the subglacial water layer has a velocity of 1396 ± 2 m s⁻¹ (Thoma et al., 2010; Tulaczyk et al.,
 318 2014).

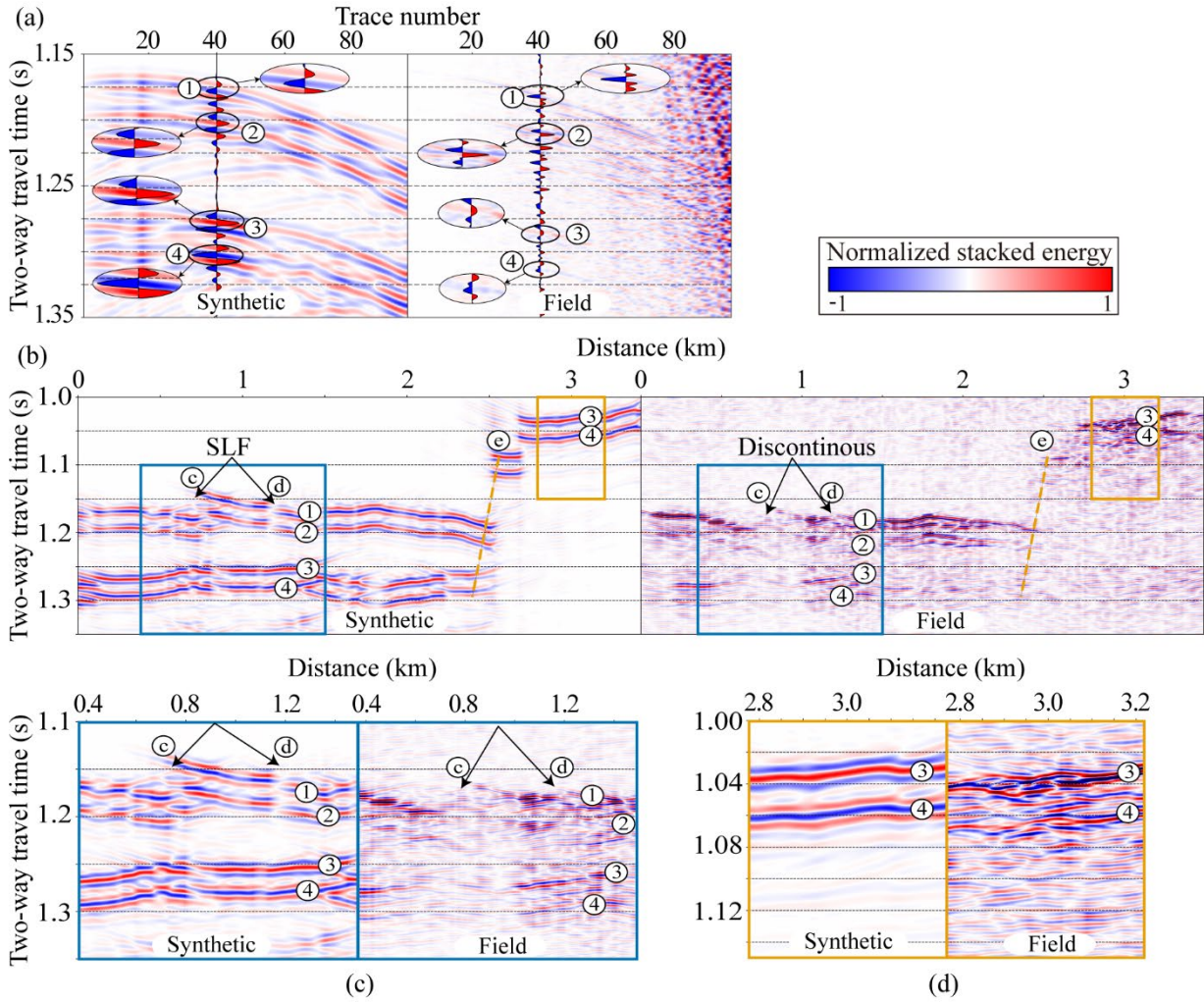
319

320 Figure 9a compares the shot gather from the synthetic dataset (left) and the corresponding gather from seismic data line 21YY
 321 (right) at the same location. A prominent reflection at a TWT of 1.17 s is observed in both datasets, corresponding to the
 322 glacier–lake interface (①). This reflection results in a high impedance contrast and reverse polarity due to the P-wave velocity
 323 difference between glacial ice and water. These features are consistent with previous observations at glacier–lake interfaces
 324 (Atre and Bentley, 1993; Brisbourne et al., 2023; Horgan et al., 2012; King et al., 2004; Peters et al., 2007; Woodward et al.,
 325 2010). A secondary reflection with normal polarity appears approximately 28 ms after the primary event (②) and is interpreted
 326 as a surface ghost reflection. This time delay corresponds to a ~~generating~~ seismic source depth of approximately 25 m, which
 327 is consistent with previous seismic analyses (Brisbourne et al., 2023; Schlegel et al., 2024). That is, assuming an average P-
 328 wave velocity of 1800 m s⁻¹ within the top 25 m, the TWT of the ghost reflection matches the expected delay:

$$329 \quad \text{TWT}_{\text{ghost}} = \frac{2 \times 25 \text{ m}}{1800 \text{ m/s}} \approx 28 \text{ ms.}$$

330





332
333 **Figure 9: Comparison of synthetic and field seismic data.** (a) Shot gather at the same location for synthetic (left) and 21YY field data (right).
334 (b) PSTM [images](#) comparison between the synthetic model and the 21YY line. (c) Enlarged views of discontinuous reflections
335 ([A-1](#): synthetic, [A-2](#): field). (d) Comparison of dipping bed reflections ([B-1](#): synthetic, [B-2](#): field), showing shadow zones and steep
336 basal topography.

337

338 Furthermore, considering that the acoustic impedance of air is approximately zero ($Z_{air} \approx 0$) and that of ice is Z_{ice} , the
339 reflection coefficient (RC) for an upgoing wave at the air–ice interface can be approximated as follows:

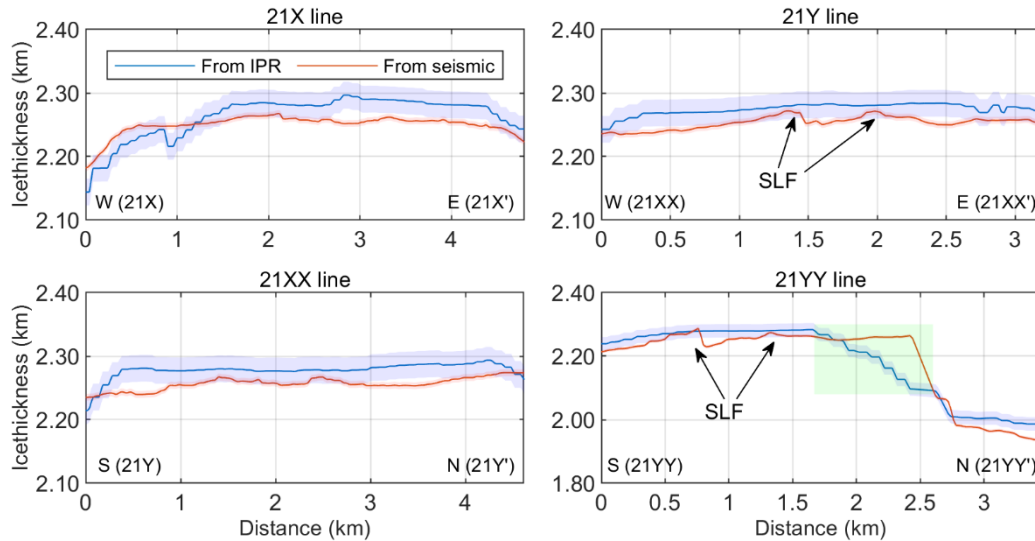
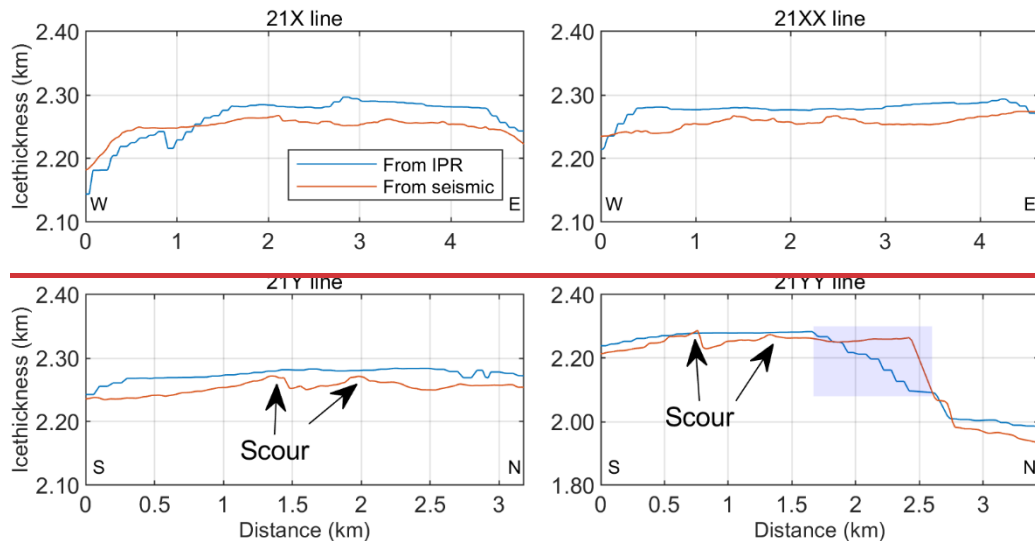
340
$$RC = \frac{Z_{air} - Z_{ice}}{Z_{ice} + Z_{air}} \approx -1. \quad (1)$$

341 This implies that the polarity of the ghost reflection at the surface is reversed relative to the downgoing primary wave (Kralj
342 and Shin, 1990; Robinson and Treitel, 2008).

343 Figure 9b compares the PSTM sections of the synthetic model (left) and the field data from line 21YY (right). Unlike the field
344 data, the synthetic dataset is free from ambient noise and features a precise source–receiver geometry, resulting in clearer

345 delineation of subsurface reflections and facilitating structural interpretation. The synthetic and field PSTM sections exhibit
346 four principal reflection events (①–④) at identical TWTs. Reflections ① and ④ are characterized by reverse polarity,
347 whereas ② and ③ display normal polarity, which is consistent across both datasets. Discontinuous reflections observed in
348 the synthetic model are interpreted as indicative of a subglacial ~~seoul~~SLF surface.
349 Figure 9c provides a magnified comparison of regions ~~A-1~~(synthetic) and ~~A-2~~(field), ~~focusing with a focus~~ on discontinuous
350 features. Although the discontinuous reflections and associated low impedance at 0.7 km and 1.2 km (TWT = 1.~~4918~~ s) in the
351 field data (~~A-2~~) are challenging to resolve, the ~~seoul~~SLF surface beneath the glacier is imaged in the synthetic section(~~A-1~~).
352 Figure 9d presents a magnified comparison of regions ~~B-1~~(synthetic) and ~~B-2~~(field) to examine reflections from a dipping
353 bed. Within 2.4–2.55 km and TWTs of ~~1.0408–1.2717~~ s, reflections are temporally dispersed, resulting in a shadow zone
354 where coherent signals are absent. From ~~0.2–0~~–2.4 km, a reversed-polarity reflection (①) is observed, whereas from 2.55–
355 ~~3.04~~ km, a normal-polarity reflection (③) is present. The latter is interpreted as the glacier–bed interface. The dashed line
356 traces the steeply dipping bed geometry, delineating the lake margin, with an estimated dip angle of approximately 52°. The
357 resulting shadow zone is likely caused by the lateral scattering of seismic energy along the steep slope. The comparison of
358 synthetic PSTM sections confirms that the velocity model used for seismic imaging appropriately represents the structures of
359 glacial and subglacial lakes.

360 To further validate the interpretation, ice thickness estimates from the seismic data were compared with those derived from
361 airborne IPR surveys along four seismic lines (Fig. 10) (~~Frémard et al., 2023;~~ Ju et al., 2024b~~5~~). Given the lack of spatial
362 coincidence between seismic and IPR profiles, kriging-based two-dimensional interpolation (Isaaks and Srivastava, 1989) was
363 applied to the IPR dataset to estimate the ice thickness at seismic line locations. The uncertainties associated with the IPR and
364 seismic datasets are ± 20.98 m and ± 5.27 m, respectively, resulting in a combined uncertainty of ± 24.05 m. The root mean
365 square error (RMSE) between the two datasets is calculated as ± 29.4 m, exceeding this expected uncertainty range. This
366 discrepancy is attributed primarily to smoothing effects introduced by interpolation in the IPR data, particularly between 1.7
367 and 2.6 km along line 21YY, within the light blue shaded area in Fig. 10, where seismic data reveal a significantly steeper
368 basal slope. When this localized region is excluded, the RMSE is reduced to ± 24.8 m, approximating the combined uncertainty.
369 Thus, apart from localized artifacts, the seismic and IPR datasets exhibit strong agreement. This consistency supports the
370 mutual reliability of both methods and validates their integrated application for subglacial lake characterization. Despite
371 localized differences, the overall ice thickness estimates from both datasets are in strong agreement, and this cross-validation
372 reinforces the robustness of the seismic interpretation and affirms the consistency between the two geophysical approaches.
373 As additional supporting evidence for ~~the~~is interpretation, a steeply dipping (approximately 52°) bedrock boundary observed
374 along the 21YY line is consistently identified in both the seismic PSTM profile (Figure 9d) and the IPR-derived ice thickness
375 graph (Figure 10), indicating a similar topographic transition in both datasets. This boundary is interpreted as a structural
376 margin delineating the lateral extent of SLD2 and likely functions as a hydrological barrier. The structural congruence observed
377 in both seismic and radar data underscores the effectiveness of integrating these datasets to delineate the boundaries of
378 subglacial lakes, particularly in regions characterized by complex basal topography.



382 Figure 10: A comparison of ice thickness estimates derived from seismic and kriging-interpolated IPR data (Frémand et al., 2023;
 383 Ju et al., 2024b⁵) along the four seismic survey lines reveals high overall consistency between the two datasets, despite localized
 384 discrepancies. The light blue shaded region in the 21YY line represents areas where interpolation contributes to the divergence
 385 between the two measurement approaches. The light blue envelope represents the uncertainty bounds associated with the IPR-
 386 derived estimates, while the light red envelope indicates uncertainty bounds for the seismic-derived estimates.

388 **6 Conclusion**

389 Since 2016, the [Korea Polar Research Institute \(KOPRI\)](#) has conducted a series of geophysical investigations to study SLD2
390 beneath David Glacier, beginning with airborne IPR surveys. In 2021, a seismic survey was carried out to characterize the
391 internal structure and water column of SLD2. The seismic data revealed strong, laterally continuous reflections with reverse
392 polarity at the glacier–lake interface, whereas normal-polarity reflections were observed at the glacier–bed and lake–bed
393 interfaces.

394 A velocity model was constructed on the basis of seismic interpretation, and synthetic seismic data were generated through
395 wave propagation modeling. A comparison between synthetic and field PSTM sections demonstrated strong agreement in the
396 timing and polarity of major reflection events at the glacier–lake and lake–bed interfaces, confirming the validity of the velocity
397 model. This model estimated the ice thickness and lake water column height to be 2250–2300 m and 53–82 m, respectively.
398 These thickness estimates are in close agreement with independent IPR measurements acquired in 2018⁵ ([Ju et al., 2025](#)),
399 further supporting the reliability of the seismic interpretation.

400 In lines 21Y and 21YY, discontinuous reflections were observed near the glacier base. The discontinuous signals are
401 interpreted as [several](#) surfaces formed by basal erosion. Structural alignment across multiple survey lines reveals that these
402 features are oriented in the direction of ice flow, supporting the interpretation of glacial erosion processes at the bed.

403 This study demonstrates the utility of seismic surveys for the structural characterization of subglacial lake environments. The
404 integrated analysis of seismic and synthetic data provides quantitative constraints on the geometry of SLD2**[beneath David](#)**
405 [Glacier. It offers critical insights for future research and logistical planning, including potential subglacial drilling operations](#)
406 [A beneath David Glacier. This study offers critical insights for future logistical planning, including potential subglacial drilling](#)
407 [operations. Ultimately, this study identifies the area within a 1 km radius of S 75.422°, W 155.441° as a suitable candidate](#)
408 [site for clean hot-water drilling, given its wide spatial extent, minimum estimated water depth exceeding approximately 50 m,](#)
409 [and absence of contamination from surface field camps. The site is therefore considered highly appropriate for future](#)
410 [exploration of active subglacial lakes. Furthermore, we plan to conduct follow-up studies incorporating advanced processing](#)
411 [techniques such as deghosting, amplitude variation with offset \(AVO\) analysis, and the development of a refined velocity](#)
412 [model that accounts for detailed firn-layer properties. These technical advancements are expected to enhance the resolution](#)
413 [and precision of seismic imaging and contribute to a deeper understanding of the subglacial environment in future](#)
414 [investigations.](#)

415 **Data availability**

416 [The ICESat-2 data used in this study are available from the National Snow and Ice Data Center \(NSIDC\).](#) The seismic data
417 and ICESat-2 laser altimetry [datasets](#) used in this study are also available through the Korea Polar Data Center
418 (KPDC) [upon request](#) at <https://dx.doi.org/doi:10.22663/KOPRI-KPDC-00001177>. The maps related to Antarctica were
419 created using the Quantarctica dataset version 3.2 (Matsuoka et al., 2018).

420 **Author contributions**

421 HJ: Writing—original draft, investigation, methodology, conceptualization. SGK: Writing—original draft, methodology,
422 conceptualization, supervision. YC: Writing – original draft, data processing, modeling. SP: Data processing methodology.
423 MJL: Writing – original draft. HK: Hot-water drilling. KK: Investigation. YK: Investigation. JIL: Project administration,
424 Funding acquisition.

425 **Competing interests**

426 The authors declare that they have no known competing financial interests or personal relationships that could have appeared
427 to influence the work reported in this paper.

428 **Acknowledgements**

429 We express our sincere gratitude to Sungjun Jeon and the K-route team for their invaluable logistical support. We also extend
430 our appreciation to Do-youn Kwon, Jamin Park, Sanghyeok Seo, and Byeongguk Moon for their dedicated assistance in
431 seismic surveys.

432 **Financial support**

433 This research was supported by KOPRI grants funded by the Ministry of Oceans and Fisheries (KOPRI project Nos. PE25070).

434 **Additional information:**

435 We name Subglacial Lake D2 Subglacial Lake Cheongsuk (SLC). The name Cheongsuk has a significant meaning, as it is the
436 pen name of Dr. Yeadong Kim, the founder of the [Korea Polar Research Institute \(KOPRI\)](#) and former president of the
437 Scientific Committee on Antarctic Research (SCAR). Dr. Kim personally led the IPR and seismic surveys of Subglacial Lake
438 Cheongsuk and coauthored this paper.

439

440 **Financial support**

441 This research was supported by KOPRI grants funded by the Ministry of Oceans and Fisheries (KOPRI project Nos. PE25070).

442

443 **References**

444 Atre, S. R. and Bentley, C. R.: Laterally varying basal conditions beneath ice Streams B and C, West Antarctica,
445 *J. Glaciol.*, 39, 507–514, <https://doi.org/10.3189/s0022143000016403>, 1993.

446 Bell, R. E., Studinger, M., Shuman, C. A., Fahnestock, M. A., and Joughin, I.: Large subglacial lakes in East
447 Antarctica at the onset of fast-flowing ice streams, *Nature*, 445, 904–907,
448 <https://doi.org/10.1038/nature05554>, 2007.

449 Bell, R. E., Ferraccioli, F., Creyts, T. T., Braaten, D., Corr, H., Das, I., Damaske, D., Frearson, N., Jordan, T.,
450 Rose, K., Studinger, M., and Wolovick, M.: Widespread persistent thickening of the east antarctic ice sheet
451 by freezing from the base, *Science*, 331, 1592–1595, <https://doi.org/10.1126/science.1200109>, 2011.

452 Bentley, M. J., Hodgson, D. A., Smith, J. A., Cofaigh, C. Ó., Domack, E. W., Larter, R. D., Roberts, S. J.,
453 Brachfeld, S., Leventer, A., Hjort, C., Hillenbrand, C. D., and Evans, J.: Mechanisms of Holocene
454 paleoenvironmental change in the Antarctic Peninsula region, *Holocene*, 19, 51–69,
455 <https://doi.org/10.1177/0959683608096603>, 2009.

456 Brisbourne, A. M., Smith, A. M., Rivera, A., Zamora, R., Napoleoni, F., Uribe, J. A., and Ortega, M.:
457 Bathymetry and bed conditions of Lago Subglacial CECs, West Antarctica, *J. Glaciol.*, 69, 1–10,
458 <https://doi.org/10.1017/jog.2023.38>, 2023.

459 Christianson, K., Jacobel, R. W., Horgan, H. J., Anandakrishnan, S., and Alley, R. B.: Subglacial Lake Whillans
460 — Ice-penetrating radar and GPS observations of a shallow active reservoir beneath a West Antarctic ice
461 stream, *Earth Planet. Sc. Lett.*, 331–332, 237–245, <https://doi.org/10.1016/j.epsl.2012.03.013>, 2012.

462 Christner, B. C., Priscu, J. C., Achberger, A. M., Barbante, C., Carter, S. P., Christianson, K., Michaud, A. B.,
463 Mikucki, J. A., Mitchell, A. C., Skidmore, M. L., Vick-Majors, T. J., Adkins, W. P., Anandakrishnan, S.,
464 Barcheck, G., Beem, L., Behar, A., Beitch, M., Bolsey, R., Branecky, C., Edwards, R., Fisher, A., Fricker, H.,
465 Foley, N., Guthrie, B., Hodson, T., Horgan, H., Jacobel, R., Kelley, S., Mankoff, K. D., McBryan, E.,
466 Powell, R., Purcell, A., Sampson, D., Scherer, R., Sherve, J., Siegfried, M., and Tulaczyk, S.: A microbial
467 ecosystem beneath the West Antarctic ice sheet, *Nature*, 512, 310–313, <https://doi.org/10.1038/nature13667>,
468 2014.

469 Dow, C. F., Hubbard, A., Booth, A. D., Doyle, S. H., Gusmeroli, A., and Kulessa, B.: Seismic evidence of
470 mechanically weak sediments underlying Russell Glacier, West Greenland, *Ann. Glaciol.*, 54, 135–141,
471 <https://doi.org/10.3189/2013aog64a032>, 2013.

472 Engelhardt, H., Humphrey, N., Kamb, B., and Fahnestock, M.: Physical conditions at the base of a fast moving
473 Antarctic ice stream, *Science*, 248, 57–59, <https://doi.org/10.1126/science.248.4951.57>, 1990.

474 Filina, I. Y., Blankenship, D. D., Thoma, M., Lukin, V. V., Masolov, V. N., and Sen, M. K.: New 3D bathymetry
475 and sediment distribution in Lake Vostok: implication for pre-glacial origin and numerical modeling of the
476 internal processes within the lake, *Earth Planet. Sc. Lett.*, 276, 106–114,
477 <https://doi.org/10.1016/j.epsl.2008.09.012>, 2008.

478 Frémand, A. C., Fretwell, P., Bodart, J. A., Pitchard, H. D., Aitken, A., Bamber, J. L., Bell, R., Bianchi, C.,
479 Bingham, R. G., Blankenship, D. D., Casassa, G., Catania, G., Christianson, K., Conway, H., Corr, H. F. J.,
480 Cui, X., Damaske, D., Damm, V., Drews, R., Eagles, G., Eisen, O., Eisermann, H., Ferraccioli, F., Field, E.,
481 Forsberg, R., Franke, S., Fujita, S., Gim, Y., Goel, V., Gogineni, S. P., Greenbaum, J., Hills, B., Hindmarsh,
482 R. C. A., Hoffman, A. O., Holmlund, P., Holschuh, N., Holt, J. W., Horlings, A. N., Humbert, A., Jacobel, R.
483 W., Jansen, D., Jenkins, A., Jokat, W., Jordan, T., King, E., Kohler, J., Krabill, W., Kusk-Gillespie, M.,
484 Langley, K., Lee, J., Leitchenkov, G., Leuschen, C., Luyendyk, B., MacGregor, J., MacKie, E., Matsuoka,
485 K., Morlighem, M., Mouginot, J., Nitsche, F. O., Nogi, Y., Nost, O. A., Paden, J., Pattyn, F., Popov, S. V.,
486 Rignot, E., Rippin, D. M., Rivera, A., Roberts, J., Ross, N., Ruppel, A., Schroeder, D. M., Siegert, M. J.,
487 Smith, A. M., Steinhage, D., Studinger, M., Sun, B., Tabacco, I., Tinto, K., Urbini, S., Vaughan, D., Welch,
488 B. C., Wilson, D. S., Young, D. A., and Zirizzotti, A.: Antarctic bedmap data: findable, accessible,
489 interoperable, and reusable (FAIR) sharing of 60 years of ice bed, surface, and thickness data, *Earth Syst.
490 Sci. Data*, 15, 2695–2710, <https://doi.org/10.5194/essd-15-2695-2023>, 2023.

491 Frezzotti, M., Tabacco, I. E., and Zirizzotti, A.: Ice discharge of eastern Dome C drainage area, Antarctica,
492 determined from airborne radar survey and satellite image analysis, *J. Glaciol.*, 46, 253–264,
493 <https://doi.org/10.3189/172756500781832855>, 2000.

494 Graves, R. W.: Simulating seismic wave propagation in 3D elastic media using staggered-grid finite differences,
495 *Bulletin of the seismological society of America*, 86, 1091–1106, <https://doi.org/10.1785/BSSA0860041091>,
496 1996.

497 Herron, D. A.: Pitfalls in seismic interpretation: depth migration artifacts, *The Leading Edge*, 19, 1016–1017,
498 <https://doi.org/10.1190/1.1438756>, 2000.

499 Horgan, H. J., Anandakrishnan, S., Jacobel, R. W., Christianson, K., Alley, R. B., Heeszel, D. S., Picotti, S., and
500 Walter, J. I.: Subglacial Lake Whillans — Seismic observations of a shallow active reservoir beneath a West
501 Antarctic ice stream, *Earth Planet. Sc. Lett.*, 331–332, 201–209, <https://doi.org/10.1016/j.epsl.2012.02.023>,
502 2012.

503 Isaaks, E. H. and Srivastava, R. M.: *An Introduction to Applied Geostatistics*, Oxford University Press, Oxford,
504 1989.

505 Johansen, T. A., Ruud, B. E., Bakke, N. E., Riste, P., Johannessen, E. P., and Henningsen, T.: Seismic profiling
506 on Arctic glaciers, *First Break*, 29, 65–71, <https://doi.org/10.3997/1365-2397.20112st1>, 2011.

507 Ju, H., Choi, Y., and Kang, S.-G.: Seismic Survey for the Subglacial Lake in Antarctica. *Geophysics and
508 Geophysical Exploration*, 27, 244–257. <https://doi.org/10.7582/gge.2024.27.4.244>, 2024a.

509 Ju, H., Kang, S., Han, H., Beem, L. H., Ng, G., Chan, K., Kim, T., Lee, J., Lee, J., Kim, Y., and Blankenship, D.
510 D.: *Air borne Ice radar survey data*Pyun, S.: *Airborne and Space borne satellite data*Spaceborne
511 *Mapping and Analysis* of *Korean route from the Subglacial Lake D2 in David glacier*Glacier, *Terra Nova*
512 *Bay*, *Antarctica in 2018* [Dataset], *J. Geophys. Res.: Earth Surf.*, 130, <https://doi.org/10.22663/kopri-kpde-00001177>, 2024b1029/2024jf008142, 2025.

514 King, E. C., Woodward, J., and Smith, A. M.: Seismic evidence for a water-filled canal in deforming till beneath
515 Rutford Ice Stream, West Antarctica, *Geophys. Res. Lett.*, 31, L20401,
516 <https://doi.org/10.1029/2004gl020379>, 2004.

517 Kirchner, J. F. and Bentley, C. R.: Seismic short-refraction studies on the Ross Ice Shelf, Antarctica, *J. Glaciol.*,
518 24, 313–319, <https://doi.org/10.3189/s0022143000014830>, 1979.

519 Kohnen, H.: The temperature dependence of seismic waves in ice, *J. Glaciol.*, 13, 144–147,
520 <https://doi.org/10.3189/s0022143000023467>, 1974.

521 Krail, P. M. and Shin, Y.: Deconvolution of a directional marine source, *Geophysics*, 55, 1542–1548,
522 <https://doi.org/10.1190/1.1442805>, 1990.

523 Lindzey, L. E., Beem, L. H., Young, D. A., Quartini, E., Blankenship, D. D., Lee, C.-K., Lee, W. S., Lee, J. I.,
524 and Lee, J.: Aerogeophysical characterization of an active subglacial lake system in the David Glacier
525 catchment, Antarctica, *Cryosphere*, 14, 2217–2233, <https://doi.org/10.5194/tc-14-2217-2020>, 2020.

526 Livingstone, S. J., Li, Y., Rutishauser, A., Sanderson, R. J., Winter, K., Mikucki, J. A., Björnsson, H., Bowling, J.
527 S., Chu, W., Dow, C. F., Fricker, H. A., McMillan, M., Ng, F. S. L., Ross, N., Siegert, M. J., Siegfried, M.,
528 and Sole, A. J.: Subglacial lakes and their changing role in a warming climate, *Nature Reviews Earth &*
529 *Environment*, 3, 106–124, <https://doi.org/10.1038/s43017-021-00246-9>, 2022.

530 Matsuoka, K., Skoglund, A., Roth, G., de Pomereu, J., Griffiths, H., Headland, R., Herried, B., Katsumata, K., Le
531 Brocq, A., Licht, K., Morgan, F., Neff, P., Ritz, C., Scheinert, M., Tamura, T., Van de Putte, A., van den
532 Broeke, M., von Deschwanden, A., Deschamps-Berger, C., ... Melvær, Y.: Quantarctica [Dataset].
533 Norwegian Polar Institute. <https://doi.org/10.21334/NPOLAR.2018.8516E961>, 2018.

534 Oliveira, M. S., Henriques, M. V. C., Leite, F. E. A., Corso, G., and Lucena, L. S.: Seismic denoising using
535 curvelet analysis, *Physica A*, 391, 2106–2110, <https://doi.org/10.1016/j.physa.2011.04.009>, 2012.

536 Peters, L. E., Anandakrishnan, S., Alley, R. B., and Smith, A. M.: Extensive storage of basal meltwater in the
537 onset region of a major West Antarctic ice stream, *Geology*, 35, 251–254, <https://doi.org/10.1130/g23222a.1>,
538 2007.

539 Picotti, S., Vuan, A., Carcione, J. M., Horgan, H. J., and Anandakrishnan, S.: Anisotropy and crystalline fabric of
540 Whillans Ice Stream (West Antarctica) inferred from multicomponent seismic data, *J. Geophys. Res. Sol.*
541 *Ea.*, 120, 4237–4262, <https://doi.org/10.1002/2014jb011591>, 2015.

542 Priscu, J. C. and Christner, B. C.: Earth's icy biosphere, in: *Microbial Diversity and Bioprospecting*, edited by:
543 Bull, A. T., ASM Press, Washington, D.C, 130–145, <https://doi.org/10.1128/9781555817770.ch13>, 2003.

544 Qin, L., Qiu, H., Nakata, N., Booth, A., Zhang, Z., Karplus, M., McKeague, J., Clark, R., and Kaip, G.: High-
545 resolution characterization of the firn layer near the West Antarctic ice sheet divide camp with active and
546 passive seismic data, *Geophys. Res. Lett.*, 51, e2024GL108933, <https://doi.org/10.1029/2024gl108933>, 2024.

547 Rignot, E., Mouginot, J., Scheuchl, B., van den Broeke, M., van Wessem, M. J., and Morlighem, M.: Four
548 decades of Antarctic Ice Sheet mass balance from 1979-2017, *P. Natl. Acad. Sci. USA*, 116, 1095–1103,
549 <https://doi.org/10.1073/pnas.1812883116>, 2019.

550 Robinson, E. A. and Treitel, S.: Digital Imaging and Deconvolution, Society of Exploration Geophysicists, Tulsa,
551 Okla, 2008.

552 Rose, K. E.: Characteristics of ice flow in Marie Byrd Land, Antarctica, *J. Glaciol.*, 24, 63–75,
553 <https://doi.org/10.3189/s0022143000014659>, 1979.

554 Schlegel, R., Brisbourne, A. M., Smith, A. M., Booth, A. D., Murray, T., King, E. C., and Clark, R. A.:
555 Subglacial bedform and moat initiation beneath Rutford Ice Stream, West Antarctica, *Geomorphology*, 458,
556 109207, <https://doi.org/10.1016/j.geomorph.2024.109207>, 2024.

557 Siegfried, M. R. and Fricker, H. A.: Thirteen years of subglacial lake activity in Antarctica from multi-mission
558 satellite altimetry, *Ann. Glaciol.*, 59, 42–55, <https://doi.org/10.1017/aog.2017.36>, 2018.

559 Smith, A. M., Woodward, J., Ross, N., Bentley, M. J., Hodgson, D. A., Siegert, M. J., and King, E. C.: Evidence
560 for the long-term sedimentary environment in an Antarctic subglacial lake, *Earth Planet. Sc. Lett.*, 504, 139–
561 151, <https://doi.org/10.1016/j.epsl.2018.10.011>, 2018.

562 Smith, B. E., Fricker, H. A., Joughin, I. R., and Tulaczyk, S.: An inventory of active subglacial lakes in
563 Antarctica detected by ICESat (2003–2008), *J. Glaciol.*, 55, 573–595,
564 <https://doi.org/10.3189/002214309789470879>, 2009.

565 [Smith, B. E., Fricker, H. A., Gardner, A. S., Medley, B., Nilsson, J., Paolo, F. S., Holschuh, N., Adusumilli, S.,
566 Brunt, K., Csatho, B., Harbeck, K., Markus, T., Neumann, T., Siegfried, M. R., and Zwally, H. J.: Pervasive
567 ice sheet mass loss reflects competing ocean and atmosphere processes, *Science*, 368, 1239–1242,
568 <https://doi.org/10.1126/science.aaz5845>, 2020.](https://doi.org/10.1126/science.aaz5845)

569 Stearns, L. A., Smith, B. E., and Hamilton, G. S.: Increased flow speed on a large East Antarctic outlet glacier
570 caused by subglacial floods, *Nat. Geosci.*, 1, 827–831, <https://doi.org/10.1038/ngeo356>, 2008.

571 Thoma, M., Grosfeld, K., Smith, A. M., and Mayer, C.: A comment on the Equation of State and the freezing
572 point equation with respect to subglacial lake modelling, *Earth Planet. Sc. Lett.*, 294, 80–84,
573 <https://doi.org/10.1016/j.epsl.2010.03.005>, 2010.

574 Tulaczyk, S., Mikucki, J. A., Siegfried, M. R., Priscu, J. C., Barcheck, C. G., Beem, L. H., Behar, A., Burnett, J.,
575 Christner, B. C., Fisher, A. T., Fricker, H. A., Mankoff, K. D., Powell, R. D., Rack, F., Sampson, D.,
576 Scherer, R. P., and Schwartz, S. Y.: WISSARD at Subglacial Lake Whillans, West Antarctica: scientific
577 operations and initial observations, *Ann. Glaciol.*, 55, 51–58, <https://doi.org/10.3189/2014aog65a009>, 2014.

578 Voigt, D. E., Peters, L. E., and Anandakrishnan, S.: ‘Georods’: the development of a four-element geophone for
579 improved seismic imaging of glaciers and ice sheets, *Ann. Glaciol.*, 54, 142–148,
580 <https://doi.org/10.3189/2013aog64a432>, 2013.

581 Wingham, D. J., Siegert, M. J., Shepherd, A., and Muir, A. S.: Rapid discharge connects Antarctic subglacial
582 lakes, *Nature*, 440, 1033–1036, <https://doi.org/10.1038/nature04660>, 2006.

583 Winsborrow, M. C. M., Clark, C. D., and Stokes, C. R.: What controls the location of ice streams?, *Earth-Sci.
584 Rev.*, 103, 45–59, <https://doi.org/10.1016/j.earscirev.2010.07.003>, 2010.

585 Woodward, J., Smith, A. M., Ross, N., Thoma, M., Corr, H. F. J., King, E. C., King, M. A., Grosfeld, K., Tranter,
586 M., and Siegert, M. J.: Location for direct access to subglacial Lake Ellsworth: an assessment of geophysical
587 data and modeling, *Geophys. Res. Lett.*, 37, L11501, <https://doi.org/10.1029/2010gl042884>, 2010.

588 Wright, A. and Siegert, M.: A fourth inventory of Antarctic subglacial lakes, *Antarct. Sci.*, 24, 659–664,
589 <https://doi.org/10.1017/s095410201200048x>, 2012.

590 Yan, S., Blankenship, D. D., Greenbaum, J. S., Young, D. A., Li, L., Rutishauser, A., Guo, J., Roberts, J. L., van
591 Ommen, T. D., Siegert, M. J., and Sun, B.: A newly discovered subglacial lake in East Antarctica likely
592 hosts a valuable sedimentary record of ice and climate change, *Geology*, 50, 949–953,
593 <https://doi.org/10.1130/g50009.1>, 2022.

594 Yilmaz, Ö.: *Seismic Data Analysis: Processing, Inversion, and Interpretation of Seismic Data*, Society of
595 Exploration Geophysicists, Tulsa, Okla, 2001.

596 Zechmann, J. M., Booth, A. D., Truffer, M., Gusmeroli, A., Amundson, J. M., and Larsen, C. F.: Active seismic
597 studies in valley glacier settings: strategies and limitations, *J. Glaciol.*, 64, 796–810,
598 <https://doi.org/10.1017/jog.2018.69>, 2018.